



## DIPLOMARBEIT

# Study and Analysis of reactor core configurations of TRIGA Mark II with SERPENT calculation code

Zur Erlangung des akademischen Grades

**Diplom-Ingenieur/in**

im Rahmen des Studiums

**Physikalische Energie- und Messtechnik**

eingereicht von

**Eva-Maria Furtmüller**

Matrikelnummer: 01225967

ausgeführt am Atominstitut  
der Fakultät für Physik der Technischen Universität Wien

Betreuung

Betreuer/in: Ao. Univ. Prof. Dr. Helmuth Böck

Mitwirkung: Marcella Cagnazzo, PhD.

Wien, 17.01.2019

\_\_\_\_\_  
(Unterschrift Verfasser/in)

\_\_\_\_\_  
(Unterschrift Betreuer/in)

# Zusammenfassung

Das Ziel dieser Arbeit ist es, die zeitliche Entwicklung der Brennstoffzusammensetzung im neuen Reaktorkern des TRIGA Mark II Reaktors richtig abzuschätzen und allfällige Ergebnisse mit denen bereits durchgeführter Reaktivitätsmessungen mit den jeweiligen Kernkonfigurationen zu vergleichen. Um das umsetzen zu können, wird ein erst kürzlich entwickeltes Programm namens SERPENT verwendet, welches auf Monte Carlo Basis für kontinuierliche Energien reaktorphysikalische Burnup Berechnungen durchführen kann. Um die zeitliche Evolution so realitätsnah wie möglich simulieren zu können, müssen zu Beginn das erste Kritikalitätsexperiment mit dem prämierten Kern aus 2013 und anschließend die Messungen mit den darauf folgenden Kernen reproduziert werden. Im Zuge dessen wird der Programmcode für angepasste oder hinzugefügte geometrischer Elemente hinsichtlich verschiedener Ziele der Simulationen der einzelnen Kernkonfigurationen verändert. Darauf folgt die Durchführung der tatsächlichen Burnup Kalkulationen und beruhend auf deren Ergebnisse die Aktualisierung der Materialzusammensetzung der Brennelemente, um die notwendigen Kern- und Kritikalitätsparameter bestimmen und überprüfen zu können

## **Abstract**

The purpose of this Thesis is to estimate the time-evolution of the fuel composition throughout several reactor core configurations of the TRIGA Mark II reactor and compare the results with experimental values taken from historical records and performed in the actual reactor core arrangement. To achieve this, the simulations are carried out by a recently developed, continuous-energy Monte Carlo reactor physics burn-up calculation code, called Serpent. In order to simulate the time-evolution, it is necessary to reproduce the first criticality experiment performed with the initial-2013 core load and the ensuing measurements using further reactor core configurations. Therefore the code input file has to be updated for each core configuration basing on the conditions of the experiment. To being able to analyze the fuel time-evolution throughout the operation of different reactor cores burnup calculations are performed. The results are used to update the material composition of the fuel elements in all cores and eventually gain the actual core parameters.

# Danksagung

## Acknowledgement

An diese Stelle möchte ich die Chance nutzen, um mich bei allen, die mich im Laufe des Entstehens dieser Masterarbeit unterstützt haben, zu bedanken.

Allen voran gebührt dieser Dank Herrn Prof. Helmuth Böck, der mir während des ganzen Prozesses immer hilfreich zur Seite stand, geduldig meine Fragen beantwortete und einmal mehr zu meinem Mentor wurde.

Ebenfalls herzlich danken möchte ich meiner Supervisorin Marcella Cagnazzo, PhD.

*Marcella, thank you very much for supporting me during this thesis. Without your patience, knowledge and intuition, especially when it came to achieving the best possible results, this would have not turned out half as good.*

Danke an Dr. Mario Villa, der mir viele male bei der Beschaffung und Interpretation von Aufzeichnungen und Informationen geholfen hat und dem keine meiner vielen Anfragen zu dringlich war.

Zu guter Letzt möchte ich mich noch ganz besonders bei meiner Familie bedanken, die nicht nur während dieser Masterarbeit, sondern auch das ganze Studium hindurch hinter mir stand und mich mit Worten, Gesten und Obstellern stets ermutigt hat.

# Table of Content

<b>Introduction</b>	9
<b><u>Physical Background</u></b>	11
<b>1. Atomic structure and radioactivity</b>	12
1.1. Nucleus and shell of atoms	12
1.2 Nuclear binding energy and mass defect	14
1.3 Radioactive decay and interaction of ionising radiation and matter	15
1.3.1 Law of radioactive decay	15
1.3.2 Types of radioactive decay	16
1.3.2.1 Alpha decay	16
1.3.2.2 Beta decay	17
1.3.2.3 Gamma radiation	17
1.3.3. Interaction of ionising radiation and matter	18
References Chapter 1	20
<b>2. Reactor physics</b>	21
2.1 Mass defect per nucleon	22
2.2 Chain reaction	23
2.2.1 Neutron multiplication factor	24
2.3 Cross sections	25
2.3.1 Energy dependency of cross sections	26
2.3.2 Fission cross section of U-235	26
2.4 Neutrons and fission products	28
2.4.1 Thermal, prompt and delayed Neutrons	28
2.4.2 Fission products of U-235	29
2.4.3 Moderation of neutrons	30
2.4.4 Neutron poisoning	30
2.5 Criticality	32
2.5.1 Four-factor equation	32
2.5.2 Reactor period	34
	5

2.5.3 Reactivity	34
2.5.4 Inhour equation	35
2.6 Burnup	35
References Chapter 2	37
<b><u>TRIGA Mark II Reactor Vienna &amp; Serpent Code</u></b>	<b>38</b>
<b>3. Vienna TRIGA Mark II Reactor</b>	<b>39</b>
3.1 Characteristics of Vienna Mark II reactor	40
3.2 Reactor construction	41
3.3 Reactor Core	43
3.3.1 Fuel elements	44
3.3.2 Irradiation history of the fuel elements	45
3.3.3 Control Rods	46
3.3.4 Graphite dummy elements	46
3.3.5 Reactor Instrumentation	47
References Chapter 3	48
<b>4. Serpent -</b>	
<b>A Continuous-energy Monte Carlo Reactor Physics Burnup Calculation Code</b>	<b>49</b>
4.1 Geometry Input	50
4.2 Neutron Population and Criticality Cycles	50
4.3 Particle tracking	51
4.4 Burnup calculation	52
4.4.1 Output files and Burnup results	53
4.5 Data Libraries	54
4.6 Running Serpent	54
4.7 Implementation of the Serpent Reactor Model	56
4.7.1 Geometry	56
4.7.1.1 Surface and Cell Cards	58
4.7.1.2 Universes and lattice-based structure	58
4.7.1.3 Material Definitions	60
References Chapter 4	62

<b><u>Simulations &amp; Discussion of the Results</u></b>	63
<b>5. Core I, 2013-01-21 to 2013-07-22</b>	64
5.1 Update of the fuel element configuration	64
5.2 Modelling of the Control Rods	66
5.2.1 Worth of the Control Rods	66
5.2.2 Experimental calibration of a Control Rod	67
5.2.3 Simulation of the Control Rod Worth	68
5.2.4 Comparison of Simulation and experimental Data	69
5.3 Core I Excess reactivity	71
5.3.1 Experimental determination of the Core Excess Reactivity	72
5.3.2 Simulation of the Core Excess Reactivity	72
5.3.3 Comparison of Simulation and experimental Data	73
5.4 Burnup Calculation	76
5.4.1 Burnup Intensity	76
5.4.2 Calculation time intervals	78
References Chapter 5	80
<b>6. Core II and Core III, 2013-07-22 to 2014-04-14</b>	81
6.1 Update of the fuel element configuration	83
6.1.1 Changes in the fuel composition	83
6.1.2. Neutron poisons in the composition	84
6.2 Burnup Calculation	86
6.3 Worth of the Control Rods	87
6.3.1 Comparison of Simulation and experimental Data	88
6.4 Core III Excess Reactivity	89
6.4.1 Comparison of Simulation and experimental Data	90
<b>7. Core IV, 2014-04-14 to 2015-04-02</b>	92
7.1 Update of the fuel element configuration	93
7.1.1 Changes in the fuel composition	93
7.2 Burnup Calculation	94
7.3 Worth of the Control Rods	95

7.3.1 Comparison of Simulation and experimental Data	95
7.4 Core IV Excess Reactivity	96
7.4.1 Comparison of Simulation and experimental Data	97
<b>8. Burnup and Evolution of U-235</b>	99
<b>Conclusion</b>	102

# Introduction

Nuclear reactors respond particularly sensitive to any changes of crucial parameters affecting its reactivity. Therefore it is important to determine and keep track of any of these parameters and to ensure, that certain control values for the reactivity of a core configuration, i.e. the neutron multiplication factor  $k_{eff}$ , the reactor shut down margin and the core excess reactivity  $\Delta\rho$ , stay within the range of optimal reactor operation.

This thesis can be divided into three main parts, each consisting of several chapters. The first part recalls nuclear reactions and common principles of reactor physics that are relevant for the work performed in this thesis.

Reactor control parameters depend among other influences on the arrangement and number of the fuel elements in the reactor core and their amount of fissile uranium-235 nuclei. This amount decreases throughout the operation of the nuclear reactor due to fuel depletion and has to be regularly reconsidered along with the production of further isotopes. A way to calculate the changes in the composition of the fuel elements is to execute simulations of the reactor operation. The calculations for the TRIGA Mark II reactor Vienna in this thesis are performed using Serpent, a continuous-energy Monte Carlo reactor physics burn-up calculation code. The characteristics of the research reactor TRIGA Mark II Vienna and an introduction to the Serpent simulation code are featured in the second part of the thesis.

The aim of the Serpent simulations in this Master thesis is the evaluation of transmutation rates in the TRIGA Mark II reactor Vienna. This refers mainly to estimating the time-evolution of the fuel composition starting from the new core established in 2013 throughout several following core configurations. The gained simulation data undergoes comparison with reactivity measurement results taken from historical records and performed in the respective core configuration.

The starting point of this work is adapting the first core after the fuel element refuelling into Serpent and reproducing the first criticality experiment. Using the results gained from the simulation, the required benchmark data can be calculated. Comparing that

data to the values gained, when the experiment was actually performed in the reactor, enables to draw conclusions concerning the accuracy of the Serpent simulation.

As the core configuration had been in operation for a period of time the burnup of the fuel elements has to be taken into account. Once the element compositions are updated the procedure restarts with building the following core and running the experiments to gain benchmark data. The applied measurement procedures, the considerations for the simulations and the comparison of the experimental and the calculation results are presented in the third part of this thesis.

This work covers the time period from January 2013 to April 2015 and the simulations of four different core configurations. An agreement between the calculation and the measurement results validates the use of Serpent for the TRIGA Mark II reactor Vienna and makes it possible to analyze future core configurations by their reactivity parameters before actually implementing them into the reactor core.

# **Physical Background**

# 1.

## Atomic structure and radioactivity

Using adequate simulations is key to being able to predetermine essential parameters, which allow controlled operation of nuclear reactors. To understand the importance of these parameters, it is essential to know the physical processes happening within the reactor and their behavior under certain influences.

### 1.1. Nucleus and shell of atoms

Atoms consist of a nucleus and an atomic shell. The atomic shell comprises electrons and is charged negatively. It hardly holds any share of the atomic mass, but defines the atomic radius, which is in the range of a few Ångström ( $\text{Å}=10^{-10}\text{m}$ ). [1] The very compact atomic nucleus makes up for 99.9% of the atom's entire mass, consists of protons and neutrons, so-called *nucleons*, and is positively charged. Nucleons are held in association by short-ranged nuclear strong force. Atomic shell and nucleus are bound together by electromagnetic force, due to the opposite electric charge.

In electrically neutral atoms the numbers of electrons and protons are identical and called atomic number  $Z$ . The sum of the amount of protons  $Z$  and the number of neutrons  $N$  is defined as the atomic mass number  $A$ :

$$A = Z + N \quad (1.1)$$

The radius of the atomic nucleus is approximately given by

$$r_c = r_0 A^{\frac{1}{3}}, \quad (1.2)$$

with  $r_0 \approx 1.2 \text{ fm}$ . [2] Equation (1.2) indicates that the volume of the nucleus is proportional to  $A$ . This applies to the mass of the nucleus as well and suggests that the densities of all Nuclei are the same.

The stability of a nucleus is defined by the ratio of its number of protons and neutrons. This ratio changes for stable nuclei throughout the increase of the atomic mass number  $A$  in favor of the neutrons, as shown in Figure 1.1.

The most stable configuration for a light nucleus  $A \leq 30$  consists of an equal amount of neutrons and protons. This is a result of the urge to remain in the state of lowest energy and the Pauli Exclusion Principle for fermions. The Exclusion Principle states, that identical fermions (each spin  $\frac{1}{2}$ ) cannot occupy the same quantum state at the same time. Consequently a nucleus consisting of  $n$  neutrons requires the quantum state system to hold  $n$  levels of energy, one for each neutron. This behaviour changes, when nucleons consist of an equal number of neutrons and protons. As the fermions are not identical any more, each energy level can be occupied by one proton and one neutron simultaneously, making  $\frac{n}{2}$  energy levels sufficient for the whole quantum state system.[3]

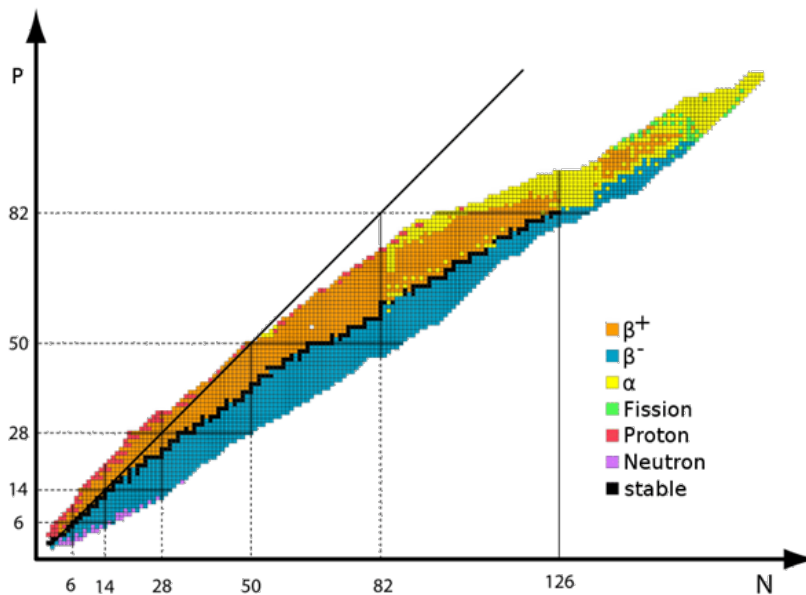


Figure 1.1: Stable elements as a function of neutrons (x-axis) and protons (y-axis). The straight line through the origin indicates  $N=P$ .

For heavier nuclei  $A > 30$  Coulomb interaction has to be taken into account. Due to their same electrical charge, protons repel each other, reducing the Nuclei stability. To counter the repulsion and assure the stability, nuclear strong force needs to increase more steeply than Coulomb force. Therefore a rising number of protons demands an even higher amount of neutrons in the nucleus. The ratio is shifted from 1:1 for  $A \leq 30$

to 1:1,6 for  $A=250$ . This compensation only works for nuclei up to  $A \leq 290$  and  $Z \leq 83$ . Any nucleus heavier than that is not stable anymore and results in a fission process.[4]

## 1.2 Nuclear binding energy and mass defect

The physical parameter majorly determining the stability of a nucleus is its binding energy per nucleon  $E_B/A$ .  $E_B$  is defined as the necessary amount of energy, needed to split a nucleus into its nucleons. It depends on certain factors considered in Bethe-Weizsäcker's semi-empirical mass formula. The most impacting factor is the ratio of surface to volume of a nucleus. A decreasing ratio suggests a higher amount of direct neighbors to each nucleon. That leads to a rise of binding energy  $E_B$ , due to the additional nuclear strong force. Regarding all stable elements  $E_B/A$  has its maximum at  $A=56$ . This results in ferric being the tightest bound and most stable element, as displayed in Figure 1.2. After a certain number of nucleons is being exceeded ( $A > 60$ ), the growing repulsion between protons starts to steadily mitigate the binding energy again.[5]

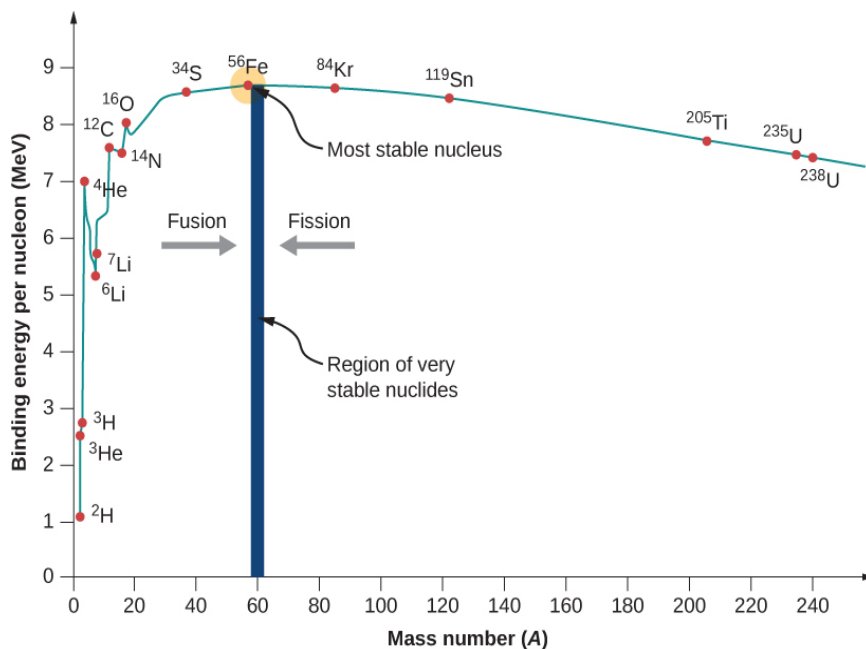


Figure 1.2: Binding energy per nucleon

In order to characterize nuclear binding energy, it is essential to have a close look on the principle of nuclear mass defect. It is based on the equality of energy and mass

$$E = mc^2 \quad (1.3)$$

and constitutes, that the mass of a nucleus ( $M_a$ ) accounts for less than the sum of its integral nucleons' masses

$$\Delta M = Zm_p + Nm_N - M_a. \quad (1.4)$$

This principle suggests, that parts of the nucleons' masses are converted into binding energy, when they assemble to build a nucleus. Multiplying  $\Delta M$  with  $c^2$  gives  $E_B$ , which is the amount of energy, that has to be put into the system to crack the nuclear configuration and split into its integral parts.[6]

Regarding power generation, there are two ways of approaching the most stable nucleus at  $A = 56$ . The gained nuclear binding energy is in the range of  $10^{-13}$ J per nucleon, as shown in figure 1.2.[4]

The first possibility is to merge several light nuclei on condition that the newly formed consists of approximately 56 nucleons. The difficulty of this endeavour called *nuclear fusion*, lies within overcoming the Coulomb repulsion of protons. This requires crucial amounts of energy, until their spatial distance is small enough for nuclear strong-force to take over. Once it does though, binding energy is being released.

The second option to gaining binding energy approaches  $A = 56$ , starting from originally very heavy nuclei. External energy input provides the necessary energy to initialize deformation vibrations, which lead to a temporary increase in repelling force between protons. The value of this force surpassing the value of the binding force between nucleons results in a *nuclear fission* process. Thereby an instable, heavy nucleus is split into two or more lighter ones. Each of it is bound more tightly than the original nucleus and binding energy is being released.

This thesis will be focussing on the nuclear fission process only.

## **1.3 Radioactive decay and interaction of ionising radiation and matter**

### **1.3.1 Law of radioactive decay**

Radioactivity characterizes the property of instable nuclei to either become another nucleus by emitting particles (i.e.  $\beta^-$ ,  $\beta^+$ ,  $\alpha$ ,  $n$ ), or to change their current quantum state

through emission of energy. Speaking more generally, it describes the transition of a nucleus under emission of ionising radiation.[2]

Radioactive decay happens to be a random and statistical process. It can be calculated with exponential decline. Supposed that there exists an amount of  $n$  radioactive nucleons at a certain time  $t$ , the number of those decaying within a time interval  $dt$  is proportional to both  $n$  and  $dt$ . The disintegrations lead to a declining amount of radioactive nuclei, following

$$dn = -\lambda n dt. \quad (1.5)$$

$\lambda$  is called *decay constant*. Integrating (1.5) and applying the exponential function on both sides of the equation, results in

$$\frac{n}{n_0} = e^{-\lambda t}. \quad (1.6)$$

$n_0$  represents the initial number of nuclei at the time  $t = 0$ . [3]

Further essential characteristics of a radioactive nucleus are the *mean lifetime*  $\tau$ , defined as the reciprocal of the decay constant  $\lambda$  and its *half-life*  $\tau_{1/2}$ . The mean lifetime and the half-life describe how long it takes to decrease the amount of nuclei either to a factor of  $e^{-1}$ , or to a factor of  $\frac{1}{2}$  of their original quantities.

### 1.3.2 Types of radioactive decay

Instable nuclei have different options of decaying, depending on their properties. There are three essential transformation processes to be distinguished.

#### 1.3.2.1 Alpha decay

Alpha radiation is a particular form of particle radiation. Very heavy and therefore instable nuclei decay by emitting so-called alpha particles, doubly-ionized He nuclides. They consist of two protons and two neutrons each, resulting in reducing the atomic mass number (A) of the parent nuclei (X) by four and its atomic number (Z) by two. During the transition into the daughter nuclide energy is released.[2]



Alpha radiation is a highly ionizing, but very short ranging form of particle radiation. Its penetration-depth is limited to a few cm. Once it is incorporated though, it can cause major damage to the body, due to its high linear energy transfer. Linear energy transfer (LET) describes the amount of energy per unit distance transferred to the material, when being pervaded by an ionized particle. It can be considered as a measurement of the amount of ionisation processes per unit distance and therefore provides information about the effectiveness of the radiation on biological tissue.

### 1.3.2.2 Beta decay

Similar to alpha decay, beta decay releases corpuscles as well. According to the type of emitted particle, two forms of decay can be differentiated:  $\beta^-$  and  $\beta^+$ -radiation.

Nuclides with a vast number of neutrons prefer to transition into an isotope of the subsequent element of the periodic table through  $\beta^-$ -decay. In this process one of the neutrons is turned into a proton and thus emits an electron and an anti-neutrino. The mass number of the parent nuclide remains unaffected, while its atomic number increases by one.



During  $\beta^+$ -decay an excess proton is converted into a neutron. Therefore a positron and an electron-neutrino are released. This process doesn't change the mass number of the nucleus either, but in difference to  $\beta^-$ -decay,  $\beta^+$ -radiation reduces the atomic number by one count. Thus the parent nucleus performs a transition into an isotope of the previous element.



The majority of the created nuclei occur in excited states and continuously emit  $\gamma$ -radiation when relaxing back to their ground states. Beta radiation has a range of a few meters in air and is able to penetrate the skin.[5]

### 1.3.2.3 Gamma radiation

Gamma radiation is a form of electro-magnetic radiation that is emitted during the transition of an excited nucleus into its ground state. In many cases gamma radiation

occurs alongside alpha and beta decay, which often leave the daughter nuclides on a higher energetic level. The excited nuclei relax back into their more stable and energetically favourable ground states by releasing radiation. The energy of the emitted  $\gamma$ -radiation is equal to the difference in between the higher and the lower energy level- typically above 200keV. For each known nucleus the energy levels are discrete and well defined. Thus the measurement of the gamma radiation's characteristic energy allows withdrawing a conclusion about the examined radionuclide.

Unlike the charged corpuscles of alpha and beta radiation, the electro-magnetic radiation's interacting particle called photon, remains uncharged. The relatively weak interaction allows gamma rays to deeply penetrate tissue and matter. The radiation intensity decreases exponentially with the penetration depth, which depends on the radiation's energy and the proton number of the absorber material.

According to the energy of the photon  $E = h\nu$  one of three interaction processes takes action.

### 1.3.3. Interaction of ionising radiation and matter

- Ionization:

Alpha and Beta particles mostly interact with matter by transferring some of their energy onto an electron bound in the atomic structure. Supposedly the amount of energy is sufficient, the electron can abandon its shell and leave the atom ionized.

- Photoelectric ionisation:

High-energy photons are being completely absorbed by an atom and their energy gets transferred to a tightly bound electron. If the amount of transferred energy is bigger than the binding energy ( $E_B$ ) of the electron, the particle can escape its atomic shell. The set free electron holds the energy difference  $h\nu - E_B$ . The vacant position in the inner shell of the ionized atom is being filled up by either repositioning the electrons in the remaining shells, or by non-radiant transitions of an electron originally located in an outer shell. Each option either releases x-rays or an auger-electron with the energy  $E_B$ . The cross-section for photoionization strongly depends on the proton number and is inversely proportional to the radiation energy:  $\sigma \propto Z^5 E_\gamma^{-3.5}$ . As a consequence, elements

with high atomic numbers- especially lead ( $Z=82$ )- are able to absorb (gamma-) radiation more efficiently. Therefore they are preferred materials for both absorbers and radiation detectors.

- Compton scattering:

Compton scattering is the main process for photon energies ranging from 0.1 to 10 MeV. A photon collides elastically with an electron at rest and thus transfers a part of its energy onto the electron. The photon itself changes its path according to the scattering angle  $\varphi$ , which is crucial to determine the amount of energy actually transmitted. Considering  $E = h \frac{c}{\lambda}$ , a reduction in the photonic energy results in a decrease of its wavelength as a function of  $\varphi$ .

- Pair production:

Photons with energies in the range of MeV or higher can be converted into an electron-positron pair, when entering the Coulomb field of an atomic nucleus. The key prerequisite here is, that the photon energy has to be at least 1.02 MeV. This is twice the rest energy of an electron. In the course of this process the photon disappears completely and all the remaining energy contributes to the kinetic energy of the electron and positron. The reverse procedure, where an electron and a positron obliterate each other and two gamma photons are emitted, is called Annihilation.[3]

## References Chapter 1

- [1] Demtröder, W.: Experimentalphysik 3, Kaiserslautern 2009  
ISBN 978-3-642-03910-2
  
- [2] Tipler, P., Mosca G.: Physik für Wissenschaftler und Ingenieure, Heidelberg 2009  
ISBN 978-3-8274-1945-3
  
- [3] Demtröder, W.: Experimentalphysik 4, Kaiserslautern 2010  
ISBN 978-3-642-01597-7
  
- [4] Lamarsh, J.: Introduction to Nuclear Engineering. Prentice Hall 2001  
ISBN 0-201-82498-1
  
- [5] Bethge, K.: Kernphysik, Heidelberg 2001  
ISBN 978-3-540-74566-2
  
- [6] Villa, M.: Vorlesungsskriptum Reaktorphysik, Technische Universität Wien 2017  
AIAU 98402

## 2.

### Reactor physics

The previously introduced nuclear fission process provides access to a great number of application opportunities, covering lots of different scientific fields. The most important technical realizations are nuclear reactors. Depending on its design, the major purpose of a nuclear reactor can range from the production of isotopes for medical treatment or neutrons for scientific research, offering an alternative propulsion system, to gaining electricity in big scale at nuclear power plants. In either case the aim is to initiate a controlled chain reaction, which continually splits heavy nuclei and gains energy and fission products in every single step.

Each transition of a nucleus is a result of a former core reaction. That reaction can either be caused by a spontaneous fission process with no need of external impact or by interaction with another particle. There are two possible outcomes for a particle hitting an atomic nucleus:

Option one suggests, that the nucleus will absorb it and subsequently emit one or more other particles. The other possibility states, that the particle will be scattered either elastically or inelastically. After inelastic scattering the nucleus remains in an excited state and decays by emitting photons or other corpuscles.

Each of these reactions either requires or releases a certain amount of energy  $Q = \Delta mc^2$ . A reaction, where the sum of the reactants' masses is bigger than the total mass of the products afterwards, releases energy. It is called *exothermic* reaction. Within the course of an *endothermic* reaction, energy has to be put into the system. The total mass of the products is bigger than the added masses of the particles stepping into the reaction. The threshold value of energy required to enable an endothermic reaction, is usually brought into the system by colliding a particle with a nucleus at rest. It has to be

slightly larger than  $|Q|$ , to ensure that the new particles hold a certain amount of kinetic energy and obey the conservation of momentum.[1]

## 2.1 Mass defect per nucleon

Nuclear reactors gain energy through approaching the most stable configuration ( $A = 56$ ) by splitting very heavy nuclei with relatively low binding energies. As discussed above, the energy set free emerges as a result of the difference in binding energy of the original and the realised nucleus.

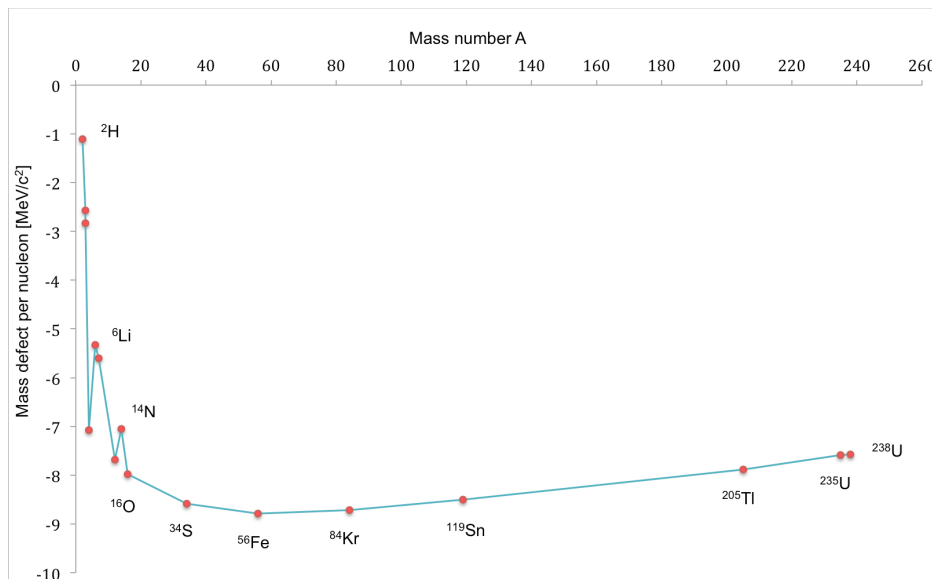


Figure 2.1: Mass defect per nucleon for nuclei with different mass numbers

The amount of released energy during a fission reaction depends on the mass defect  $\Delta M$  per nucleon  $A$ . It is given by

$$\frac{\Delta M}{A} = \frac{M_A - Zm_p - Nm_N}{A} \quad (2.1)$$

in  $MeV/c^2$  and states, that the mass of an atomic nucleus accounts for less than the sum of its nucleons' masses. Figure 2.1 presents the mass defect per nucleon for nuclei with varying numbers of components. It illustrates, that  $\Delta M/A$  is higher for heavy nuclei, than it is for moderately heavy ones around  $A = 60$ . Nuclei found in that region, are the most stable and tightly bound, in particular Iron with  $A = 56$ . Comparison of figure 2.1 and figure 1.2 shows, that the mass defect is equivalent to the negative binding energy  $E_B$

per nucleon. This means, that nuclei with lower binding energies hold higher mass defects and vice versa.[2]

Splitting a very heavy nucleus with low binding energy into two lighter nuclei, which have higher binding energies but lower mass defects per nucleon, releases a certain amount of thermal energy  $E = \Delta Mc^2$ .

The process becomes comprehensive, regarding the disintegration of a nucleus with  $A \approx 200$  into for instance two smaller nuclei with mass numbers around  $A \approx 100$ . As illustrated in figure 2.1 the rest energy per nucleon of the heavy “atomic core” is about 1MeV higher than those of the two lighter nuclei. This means, that for each nucleus split in this fission process about 200MeV of thermal energy are released.[1]

## 2.2 Chain reaction

In nuclear reactors the substance containing heavily fissile elements is called nuclear fuel. It hosts the fission process and other core reactions and usually consists of the Uranium-isotope  $^{235}_{92}\text{U}$  or in fewer cases of the Plutonium-isotope  $^{239}_{94}\text{Pu}$ .

The crucial factor to initializing an exothermic fission reaction is neutron capture. Regarding U-235 a captured neutron leads to the transition into a nucleus of the isotope U-236. This intermediate nucleus is left in a highly excited state, due to holding the additional binding energy and the kinetic energy of the neutron before the collision. There are three possible ways of de-excitation for the new U-236 nucleus: It can either decay by emitting an alpha particle, or relax back into its ground state by releasing gamma-radiation. The third option is the most likely one to happen. It suggests the fission of the nucleus into two lighter nuclei with very high kinetic energies, accompanied by the release of two to three fast neutrons and thermal energy.[3]

The key to initializing a nuclear fission process by colliding an U-235 nucleus and a neutron of defined energy lies within surpassing the value of the threshold energy of the reaction. When an U-235 nucleus absorbs a neutron and transforms into an excited U-236 nucleus, it gains 6,4MeV. At the same time the amount of energy necessary to enable

any fission of U-236 is 5,3MeV and is therefore much lower than the available excitation energy.

Over 99% of the naturally occurring uranium consists of  $^{238}_{92}\text{U}$ , which cannot be directly used as the fissile fuel component. After neutron capture of U-238, the excitation energy of U-239 lies beneath the threshold energy required to initialise the fission of the nucleus. The excited intermediate U-239 nucleus reaches its ground state by emitting gamma-radiation and after beta decaying twice turns into a Pu-239.[1]

### 2.2.1 Neutron multiplication factor

The nuclear fission process is accompanied by emitted thermal energy and also releases two to three fast neutrons. Each of these fast neutrons can interact with further U-235 nuclei and subsequently cause their fission, where again two or three neutrons are emitted. Thus a chain reaction is set into action.

The neutron multiplication factor  $k$  is the average amount of fast neutrons released per fission and capable of causing further fission events. Regarding U-235 the highest possible neutron multiplication factor  $k$  is 2,43. The actual value of  $k$  lies significantly underneath the maximum, because not all of the neutrons are able to actually induce fission. Some manage to escape the fissile area or might get absorbed by non-fissile nuclei of the fuel composition.

The equilibrium state described by  $k = 1$  is called *critical* and suggests that one fission event leads to one other event. The fission rate and the power of the reactor are held at a constant level.

When the multiplication factor rises to the *supercritical* state  $k > 1$ , there is no longer a balance of the number of neutrons produced and “lost” in the system. The amount of neutrons, capable of initiating nuclear fission keeps rising and leads to increasing power.

Looking at *subcritical* conditions  $k < 1$ , there is a decline in the number of neutrons that brings any chain reaction to a standstill.[4]

## 2.3 Cross sections

The probability of inducing a considered reaction between an incident and a target particle is given by the reaction's cross-section  $\sigma$ . The microscopic cross section is defined as the ratio of the actual amount of reactions per nucleus and time interval  $R$  to the intensity of the incident particles  $I$ . The latter is given by the number of particles impinging a unit area in the beam per time interval.

$$\sigma = \frac{R}{I} \quad (2.2)$$

This enables to estimate the frequency of the appearing interactions between neutrons (projectiles) and nuclei (targets).[3]

The magnitude of  $\sigma$  for neutron-nucleus reactions is deduced from the cross section of the nucleus itself  $R^2\pi$  and given in *barn* [ $b$ ].

$$1b = 10^{-24}cm^2 \quad (2.3)$$

Equation (2.2) describes the likelihood of the actual collision of projectile and target and is therefore called total collision cross section. It is additive and consists of the cross sections for various processes ensuing the collision .

$$\sigma = \sigma_s + \sigma_a = (\sigma_e + \sigma_i) + (\sigma_f + \sigma_c) \quad (2.4)$$

Once the neutron hits the nucleus, there are two possible options of interaction. Either the nucleus absorbs the neutron  $\sigma_a$  or it is being scattered  $\sigma_s$ . The scattering can either proceed elastically  $\sigma_e$  or inelastically  $\sigma_i$ , depending on the amount of kinetic energy transferred. In case of absorption two scenarios have to be taken into account. In the first one the neutron causes nuclear fission  $\sigma_f$ . The second option  $\sigma_c$  sums up the processes, where a neutron is absorbed, but does not lead to the emission of another neutron. Instead it favours  $\alpha$ - and  $\gamma$ -decay of the excited nucleus or its releasing of a proton.

Regarding a volume element of  $1cm^3$ , it is possible to extrapolate the macroscopic cross section  $\Sigma$  from knowing  $\sigma$ . The macroscopic cross section takes all nuclei  $N$  inside the volume element into account and appears in units of  $1/cm$ . Alternatively  $\Sigma$  is equal to the number of interactions a neutron faces along a distance of one cm. It therefore poses the reciprocal of the free path length  $\lambda$ .[5]

$$\Sigma = \sigma N \quad (2.5)$$

$$\Sigma = \frac{1}{\lambda} \quad (2.6)$$

### 2.3.1 Energy dependency of cross sections

The probability for each possible reaction depends on the kinetic energy the neutron holds before colliding with the nucleus. Every value of the cross sections can be assigned to a specific energy  $\sigma_x(E)$ . This allows adding up the cross-sections of the interactions described above and thus finding the total cross section belonging to a certain neutron-energy.

For most absorbing materials the cross section for scattering is almost negligible compared to the one for absorption. This results in shifting the total cross section towards  $\sigma_a$ , as seen in figure 2.2 for Uranium-235. Only very weakly absorbing materials have a predominant scattering cross section.

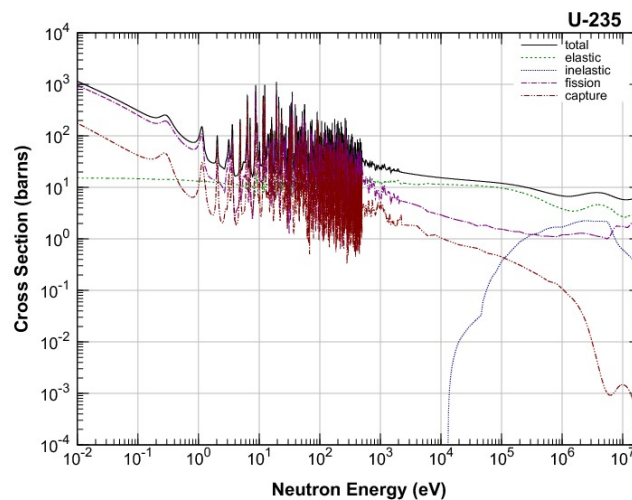


Figure 2.2: Cross sections for interactions between a neutron and a nucleus and the total cross section of U-235

### 2.3.2 Fission cross section of U-235

In order to enable induced fission the properties of U-235 must be considered. Its fission cross-section  $\sigma_f(E)$  for varying energies is depicted in figure 2.3. The function course can be divided into three sections:

For very low kinetic energies of the neutron up to 1MeV the cross section behaves proportionally to the reciprocal velocity of the particle  $\frac{1}{v}$ . The decline of the cross section for rising kinetic energy can be explained by the time the neutron spends in close proximity to the nucleus. Passing an atomic nucleus with a diameter of  $2R$  takes the neutron the time

$$t = \frac{2R}{v}. \quad (2.7)$$

The probability of absorption is proportional to the time spent close to the nucleus. The faster the neutron moves, the shorter that time gets and the cross section starts to mitigate.[1]

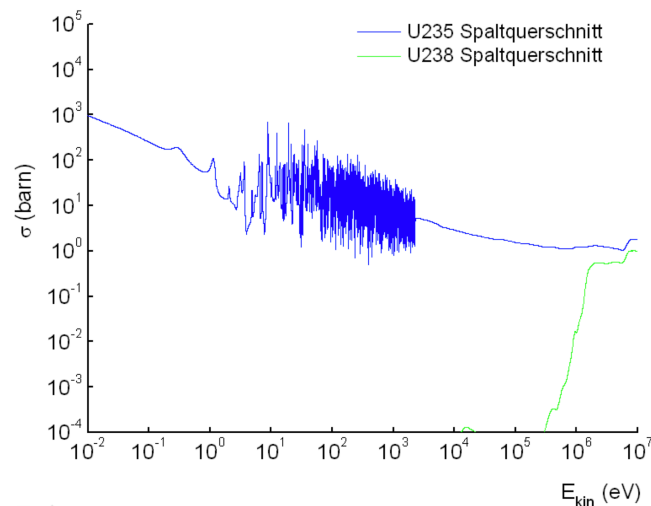


Figure 2.3: Fission cross section of U-235

The second section is called resonance range and dominates from a few eV up to 10-100keV. The sharp peaks, where the cross section rises to local maxima, are a result of the discrete energy states of the nucleus. When the sum of the neutron's binding and relative kinetic energy is equal to a discrete energy level of the nucleus, the probability of absorption increases big scale. At the same time the density of excited states rises with higher neutron energies and the distances between the single peaks are continuously reduced.

Velocities above 100keV belong to the regime of fast neutrons, which are emitted during fission. For high energies the cross section for U-235 keeps decreasing and subsequently approaches a constant level. However, the situation is different for the naturally

occurring U-238. As seen in Figure 2.3, it takes high kinetic energies and therefore fast neutrons to initialise its fission process.[5]

## 2.4 Neutrons and fission products

According to their kinetic energy and chronologic appearance different types of neutrons can be distinguished.

### 2.4.1 Thermal, prompt and delayed Neutrons

Comparatively slow neutrons have the highest chance of inducing fission of U-235 and are called *thermal* neutrons. After several scatterings those neutrons are in equilibrium with the surrounding atoms. Their energy distribution is the Maxwell-Boltzmann-distribution for the temperature of the scattering material. At room temperature the energy of thermal neutrons is usually  $k_B T \approx 0,025 \text{ eV}$ . The neutron yield per fission induced by a thermal neutron is on average 2,43.

Among the materials with the highest absorption cross-section for thermal neutrons are boron and cadmium. They are used to control the neutron flux in the absorber rods.

Another classification describes *prompt* neutrons. Those are high energetic neutrons emerging within  $10^{-14} \text{ s}$  after fission. Nearly 99% of the fission neutrons are released promptly.

*Delayed* neutrons make up 0,64% and are released after a time equal to the half-life of a beta-minus decay. The primary fission fragments are mostly instable and  $\beta^-$  decay into highly excited daughter nuclei. If the excitation energy is high enough to overcome the binding energy of the neutron, the nucleus can decay to the ground state by emitting the neutron. According to the half-life of the mother nucleus delayed neutrons can be divided into six groups. For U-235 the whole fraction  $\beta$  of delayed neutrons accounts for 0,0064. Even though that is not much, the delayed neutrons slow down the speed of the power increase significantly, which makes the reactor controllable.

Regarding both prompt and delayed neutrons, the multiplication factor  $k$  can be separated in two shares

$$k = (1 - \beta)k + \beta k. \quad (2.8)$$

The first term describes the prompt and the second term the share of delayed neutrons. As long as  $(1 - \beta)k < 1$  the reactor is controllable and can be run in normal operation mode. When  $(1 - \beta)k \geq 1$  the reactor is in a prompt critical state. That means the prompt neutrons alone are sufficient to keep the chain-reaction up. The additional neutrons would lead to an uncontrollable power excursion.[3]

### 2.4.2 Fission products of U-235

The fission of a heavy nucleus is a stochastic event. Even under the same starting conditions the distributions of occurring products differentiate strongly. Considering U-235 the primary fission fragments are highly instable and transform into another nucleus by repeated  $\beta^-$  decay. In doing so, the mass numbers stay the same and the successively arising nuclei form a chain of isobar processes towards a stable element. These stable end products of thermal nuclear fission are usually metals with mass numbers around 90 and 140. The fission product frequency distribution for U-235 is shown in Figure 2.4.

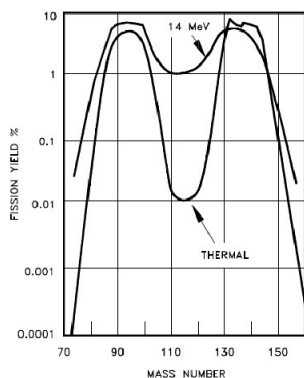


Figure 2.4: Distribution of U-235 fission products for thermal and fast neutrons

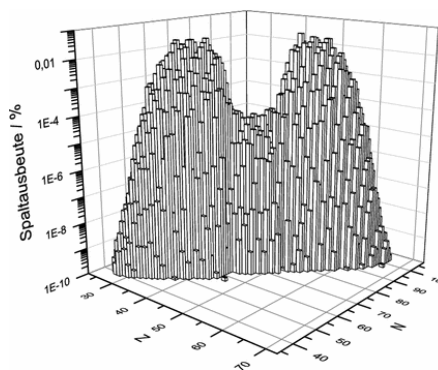


Figure 2.5: direct products of U-235 fission with thermal neutrons

As mentioned above, there are two distinct maxima at mass numbers 90 and 140 for fission with thermal neutrons. At the same time the probability of a symmetrical fission, where the products are equally big, is very low. In case that fast neutrons induce the fission, the gap between the two peaks gets filled up.[5]

Figure 2.5 displays the direct fission product yield of U-235. It gives a notion of the ratio of protons and neutrons of the fission fragments and also shows the two characteristic maxima arising from thermal fission.

### 2.4.3 Moderation of neutrons

According to the uranium-235 fission cross-section, released fast neutrons need to reduce their speed to thermal energies to initiate nuclear fission. This reduction happens by repeated *elastic* scattering against light nuclei. Energy is transferred to the nucleus and retransferred as heat after further scattering with the surrounding material. For quick deceleration good moderator materials captivate with a high loss of energy per scattering and possibly small absorption cross-sections. The most common are light water (H<sub>2</sub>O), heavy water (D<sub>2</sub>O) and graphite. The energy transferred reaches its maximum, when the mass of the two impact partners is equal. In this respect the hydrogen atom, consisting of one proton, is the preferred moderating material.

The efficiency of the different materials can be rated using

$$\xi \frac{\sigma_{el}}{\sigma_c} \tag{2.9}$$

$\xi$  represents the mean logarithmic reduction of neutron energy per collision. It takes the energy loss of the neutron per impact with a nucleus into account.  $\sigma_{el}/\sigma_c$  is the ratio of the cross-sections for elastic scattering and neutron capture. The results are demonstrated in table 2.1.[3]

Moderator	$\xi$	$\sigma_{el}$	$\sigma_c$	Rating
Light water	0.920	25.47	0.33	71
Heavy water	0.509	5.57	0.0005	5670
Graphite	0.128	5.52	0.0035	192

Table 2.1: Properties of moderating materials. Source: Wikipedia. [https://de.wikipedia.org/wiki/Moderator\\_\(Physik\)](https://de.wikipedia.org/wiki/Moderator_(Physik))

### 2.4.4 Neutron poisoning

Elements with extraordinary high cross-sections for neutron absorption are called *neutron poisons*. Some poisons are intentionally inserted into the reactor to help decreasing the number of neutrons capable of causing fission. They can also be used to

mitigate the reactivity of the initial fresh fuel load if necessary. Speaking of introducing *negative reactivity* usually refers to adding boron or control rods as poisons to the reactor core. The control rods contain neutron-absorbing elements like boron, gadolinium or cadmium to control the neutron multiplication. Other neutron poisons arise as fission products during the operation of the reactor and are both highly undesirable and inevitable. Due to their absorbing properties they may strongly influence the chain reaction and change the state of the reactor core.[6] Table 2.2 lists a few examples of neutron poisons and their associated cross-sections for thermal neutron absorption.

	<b>Xe-135</b>	<b>Gd-157</b>	<b>Sm-149</b>	<b>Cd-113</b>
$\sigma_a [cm^2]$	2650000 +/-110000	254000 +/- 815	40140 +/- 600	20600 +/- 400

Table 2.2: Absorption cross-section of a few neutron poisons. Source: IAEA.  
[http://www.iaea.org/inis/collection/NCLCollectionStore/\\_Public/34/020/34020739.pdf](http://www.iaea.org/inis/collection/NCLCollectionStore/_Public/34/020/34020739.pdf)

The isotope with the highest probability of capturing thermal neutrons is xenon-135. Its concentration is the highest during power reduction and after shutting down the reactor. It even prevents the anew power increase for a certain time. Xenon-135 is a daughter nuclide of iodine-135, which occurs during fission and has a half-life of 6,6h. When absorbing a neutron it transforms into the stable Xe-136 nucleus. In case of reactor shut down, hardly any neutrons are being released. The present I-135 still decays with the same rate to xenon though, leading to xenon poisoning as seen in figure 2.6. Its negative reactivity is so strong, that it can take one or two days until a sufficient amount of Xe-135 has decayed and the reactor can be put into operation again.

Additional to absorption cross-sections also the half-lives of the poisons have to be taken into account to judge their influence on the reactor. In a long and mid-term respect especially the cumulated poisons with a long half-life need to be considered.

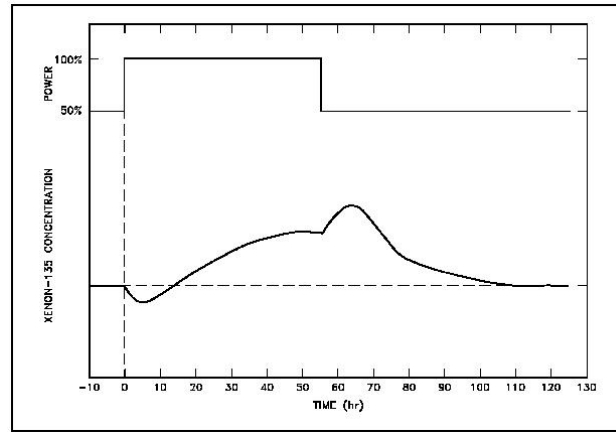


Figure 2.6: Time behavior of Xe-135 concentration

## 2.5 Criticality

### 2.5.1 Four-factor equation [3]

As discussed above the condition for criticality is to keep the chain reaction upright. That means that one neutron needs to initiate the release of at least one further neutron. In other words the number of produced neutrons has to be equal to the number of vanishing neutrons. This equilibrium state can be expressed with the neutron multiplication factor  $k = 1$  and describes a *critical* reactor.

$$k = \frac{\text{Number of neutrons belonging to generation } i}{\text{Number of neutrons belonging to generation } i - 1} = 1 \quad (2.10)$$

Regarding an infinitely large, homogenous reactor with no neutron leakage, there are four factors determining the infinite multiplication factor  $k_{\infty}$ . Each factor is independent of size and shape of the reactor and describes the average behavior of neutrons within one generation.

- The *thermal utilization factor*  $f_{th}$  provides the fraction of thermal neutrons actually absorbed by the fissile fuel component U-235 over the overall amount of neutrons absorbed.

$$f_{th} = \frac{\text{thermal neutrons absorbed by fuel isotope}}{\text{thermal neutrons absorbed anywhere}} \quad (2.11)$$

- The *reproduction factor*  $\eta_{th}$  gives the amount of fast neutrons arising after an absorbed neutron induced nuclear fission.

$$\eta_{th} = \frac{\text{neutrons produced from fission}}{\text{neutrons absorbed by fuel isotope}} \quad (2.12)$$

An absorbed thermal neutron leads in average to the release of  $f_{th}\eta_{th}$  fast neutrons.

- If the energy of a fast neutron is high enough, there is a chance that the fast neutron can lead to a fission process as well, especially regarding the U-238 isotopes in the fuel. Due to the additional fission more fast neutrons are released.

$$\varepsilon = \frac{\text{fast neutrons produced by fission at all energies}}{\text{fast neutrons produced by thermal fission}} \quad (2.13)$$

$\varepsilon$  is called *fast fission factor*.

- While the neutron is slowed down to thermal energy, there is a risk of it being absorbed by different materials or the resonances of U-238. The *resonance escape probability*  $p_{th}$  describes the chance that this will not happen.

$$p_{th} = \frac{\text{fast neutrons slowed down without getting absorbed}}{\text{total fission neutrons}} \quad (2.14)$$

The resulting  $k_{\infty}$  gives the amount of remaining thermal neutrons completing the lifecycle of one generation. Its value is solely characterized by the material composition of the reactor, i.e. uranium concentration, moderator, absorber rods, etc.

$$k_{\infty} = f_{th}\eta_{th}\varepsilon p_{th} \quad (2.15)$$

In reality the influence of neutron leakage due to finitely large reactor geometries cannot be neglected. The finite counterpart of  $k_{\infty}$  is  $k_{eff}$ , which takes two more factors into consideration.

$P_f$  and  $P_{th}$  suggest the probability, that either a fast or a thermal neutron will not leak out of the system. During reactor operation  $k_{eff}$  needs to be as close as possible to the value 1,0.

$$k_{eff} = k_{\infty}P_fP_{th} \quad (2.16)$$

### 2.5.2 Reactor period

The increase of neutrons can be described by equation (2.17).

$$\frac{dn}{dt} = \frac{n(k-1)}{\ell_0} \quad (2.17)$$

One neutron is required to keep the chain reaction going and  $\ell_0$  represents the duration of a neutron-generation. It can be calculated by dividing the free path length of absorption from equation (2.6) by an average velocity of the neutrons.

$$n = n_0 e^{\frac{(k-1)t}{\ell_0}} = n_0 e^{\frac{t}{T}} \quad (2.18)$$

Equation (2.18) introduces the *reactor period*  $T$ . It stands for the time it takes to increase the neutron flux and therefore the power of the reactor to the e-fold of its former value. Typical values of the reactor period are in the range of  $\frac{1}{10}$ s. That power excursion would be impossible to control, if it were not for the delayed neutrons. Even though they only make up for 0.64% of the neutrons in the system, they extend the reactor period about a factor of 100, which can be mechanically controlled.[3]

### 2.5.3 Reactivity

The reactivity  $\rho$  is a non-dimensional factor describing the discrepancy of the multiplication factor  $k$  from the value one.

$$\rho = \frac{k-1}{k} \quad (2.19)$$

According to its correlation to  $k$ , the reactivity characterizes the state of criticality of the reactor configuration.

- $\rho = 0$  represents  $k = 1$  and therefore a *critical* reactor.
- $\rho < 0$  is equal to  $k < 1$ . The reactor is *subcritical*
- $\rho > 0$  represents  $k > 1$ . The reactor is *supercritical*.

The deviation from criticality can be transferred into per cent mille (*pcm*), which can be seen as one one-thousandth of a percent of reactivity.

$$1pcm = \rho 10^5 \quad (2.20)$$

Taking the share of delayed neutrons  $\beta = 0,64\%$  into account, criticality can be considered in the unit dollar (\$). 1\$ is defined by normalizing equation (2.19) on the fraction of delayed neutrons  $\beta$ . It can be divided in one hundred intervals of one cent (c).

### 2.5.4 Inhour equation

Inhour is a short form of *inverse hour*, which stands for the reactivity, ensuing to keep the reactor period equal to one hour. Therefor the inhour equation constitutes the relation between reactivity and reactor period. It is visually presented in figure 2.7.

$$\rho = \frac{\ell}{kT} + \sum_i \frac{\beta_i}{\lambda_i T + 1} \quad (2.21)$$

Besides reactivity  $\rho$  and reactor period  $T$  the equation considers the neutron generation time  $\ell$ , the neutron multiplication factor  $k$ , the fraction of each group of delayed neutrons  $\beta$  and their precursor decay constant  $\lambda$ .

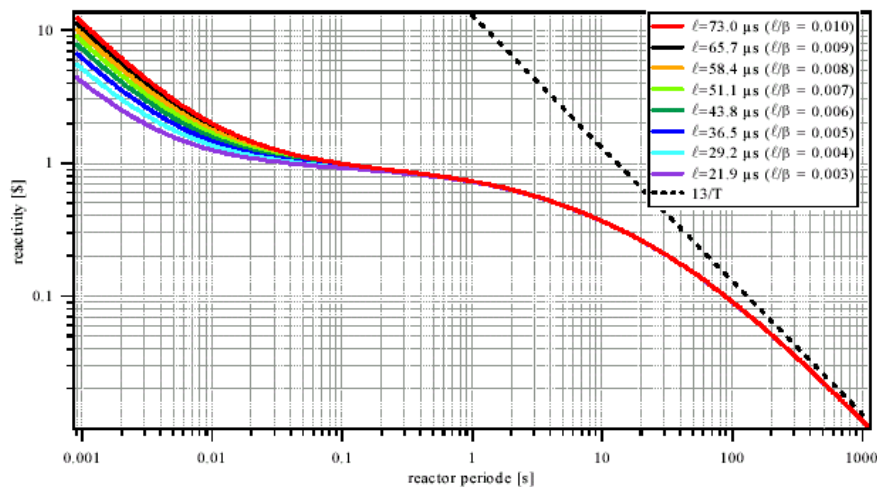


Figure 2.7: Inhour equation figure for the TRIGA reactor shows the correlation between reactor period and reactivity.

## 2.6 Burnup

The burnup in a nuclear reactor is a measurement for both the amount of thermal energy that can be extracted from the initial nuclear fuel and the fuel depletion. It can be calculated as the quotient of the thermal energy, released by the fuel up to a certain time

and the mass of the original fuel before any energy production. The result is given in  $MWd/kg$ .

$$B = \frac{E_{th}}{m} \quad (2.22)$$

Alternatively burnup can also refer to the fraction of fuel atoms in % FIMA (fission per initial metal atom) or % FIFIA (fission per initial fissile atom) that underwent fission. In that case a burnup of  $n\%$  FIMA means, that  $n\%$  of the initial amount of nuclear fuel atoms experienced fission.

## References Chapter 2

- [1] Tipler, P., Mosca G.: Physik für Wissenschaftler und Ingenieure, Heidelberg 2009  
SBN 978-3-8274-1945-3
  
- [2] Demtröder, W.: Experimentalphysik 4, Kaiserslautern 2010  
ISBN 978-3-642-01597-7
  
- [3] Villa, M.: Vorlesungsskriptum Reaktorphysik, Technische Universität Wien 2017  
AIAU 98402
  
- [4] Glasstone, S.: Principles of nuclear reactor engineering. Van Nostrand, Princeton, NJ 1955 (IX, 861).
  
- [5] Ziegler, A., Allelein, H.: Reaktortechnik: Physikalisch-technische Grundlagen, Heidelberg 2013  
ISBN 978-3-642-33845-8
  
- [6] United States Nuclear Regulatory Commission, URL:  
<https://www.nrc.gov/reading-rm/basic-ref/glossary/nuclear-poison-or-neutron-poison.html> [Date: 2018-06-26]

**TRIGA Mark II Reactor Vienna**

**&**

**Serpent Code**

### 3.

## Vienna TRIGA Mark II Reactor

The TRIGA Mark-II reactor in Vienna is a swimming-pool type research reactor, used for training, research and isotope production (*Training, Research, Isotope Production, General Atomic = TRIGA*). It was installed by General Atomic (San Diego, California, U.S.A.) in the years 1959 through 1962, and went into operation for the first time on March 7, 1962. The reactor is part of the Atominstitut, which was founded in 1958 as an inter-university institute for all Austrian universities and started operation in 1962, when the TRIGA Mark II research reactor of the institute was officially opened. In 2002 the Atominstitut was integrated into the Faculty of Physics at the TU Wien. The operation of the reactor since 1962 has averaged 220 days per year, without any long outages.[1]

The TRIGA concept had its origin in 1955 at the large international conference on the peaceful uses of atomic energy in Geneva, Switzerland. In order to forward the commercial development of nuclear reactors, General Dynamics Corporation founded the General Atomics Division (GA). A group of specialists took the challenge of creating a reactor that is safe by design, easy to operate and *“could be given to a bunch of high school children to play with, without any fear that they would get hurt.”* They accomplished their goal by utilizing UZrH-Fuel, which offers inherent safety and keeps the reactor stable during possible reactivity insertion. With growing experience GA developed five additional research reactor designs, improving and adapting the cladding, Uranium concentration and the occurring of burnable fuels. They are all part of the trademark TRIGA portfolio and share the open-pool light water moderated design, using a homogeneously mixed fuel moderator fuel element design. The neutron absorbing material in the control rods is Boron carbide.[2]

The TRIGA Mark II reactor is the most widely built type of TRIGA reactor. Its above ground design allows implementing a number of beam tubes, a thermal column and a

dry irradiation chamber.[2] The reactor tank is placed in a concrete shell, which functions as the radial irradiation shielding. The fixed core consists of some 80 fuel elements (FE), 3 control rods and several dummy graphite elements. The neutron source for this reactor is an Sb-Be photo neutron source. The core is surrounded by a graphite reflector with a depth of 30.5 cm and a height of 55.9 cm. There is a rotary specimen rack containing 40 rotating irradiation positions for experiments and storage between the core and the reflector. This rack is called *Lazy Susan*. Apart from the graphite reflector, the core is also shielded by water. In radial direction this shield is at least 45.7 cm. Over the core, the water reaches 4.9 m of height and beyond the core 61 cm. An aluminum tank and a thick borate concrete structure surround the water tank itself.[3]

### **3.1 Characteristics of Vienna Mark II reactor**

The TRIGA-reactor Vienna has a maximum continuous power output of 250 kW thermal. During normal operation mode the temperature of the fuel elements is around 200°C and the neutron-flux in the central irradiation tube amounts to  $1 \times 10^{13} \text{cm}^{-2}\text{s}^{-1}$ .

The power-controlling unit of the reactor consists of three neutron absorber rods. The control rods can be gradually inserted or removed from the core and reduce the neutron flux according to their position. If the absorber rods are withdrawn from the core the number of fissions in the core and the power level increases. The start-up process takes roughly one minute for the reactor to reach a power level of 250 kW from the sub-critical state. The reactor can be shut down either manually by inserting all three rods, or automatically by the safety system. It takes about 1/10 of a second for the control rods to fall into the core.[4]

As mentioned above, the Mark II reactor also uses uranium zirconium hydride (UZrH) fuel. The zirconium hydride serves as the main moderator and has two special and desirable properties that allow an alternative operation mode of the reactor: Firstly the moderator works less efficiently at higher temperatures. That allows a very rapid power rise up to 250 MW for roughly 40ms. This way of reactor operation is called pulsing. During a pulse the fuel temperature in the core increases to 360°C nine seconds after the

pulse and the maximum neutron flux density peaks at  $1 \times 10^{16} \text{ cm}^{-1}$ . Because of the great thermal stress the fuel is exposed to, only 12 pulses per hour are possible. The other peculiarity of the zirconium hydride moderator is its strong negative temperature coefficient of reactivity. That means, that with rising fuel temperature the reactivity decreases big scale. As a result the power level is brought back to approximately 250 kW instantly after the excursion.[5]

The heat produced is released into a channel of the river Danube via a primary and a secondary coolant circuit. The primary coolant circuit holds deionized and distilled water at temperatures between 20 and 40°C, while the secondary coolant circuit consists of ground water at temperatures between 12 and 18°C. The two circuits are being separated by a heat exchanger.[4]

### **3.2 Reactor construction**

The Mark II reactor essentially consists of an aluminum tank surrounded by a massive heavy and standard concrete shielding. The tank itself measures 1,98 m in diameter and 6,4 m in depth and is filled with ionized and distilled water. The core of the reactor is located 4,9 m underneath the water surface and has a cladding of aluminum and steel. Its active core volume makes up for 49,5 cm in diameter and 35,56 cm in height and a graphite reflector covers the whole core. The graphite is an essential part of the core's shielding, additional to the surrounding water and in radial direction at least two meters of heavy concrete. In vertical direction the core is shielded by graphite and nearly five meters of water towards the top and water, graphite and standard concrete towards the bottom. The reactor design features certain irradiation devices. Among them are four beam holes, one thermal column and an irradiation room.[5] The vertical and horizontal cross-sections of the reactor are displayed in figures 3.1 and 3.2.

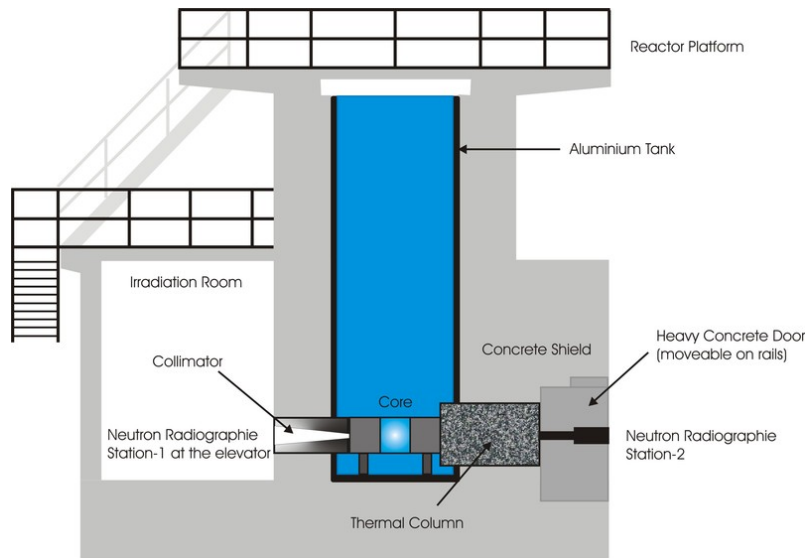


Figure 3.1: vertical cross-section of the TRIGA Mark II reactor in Vienna

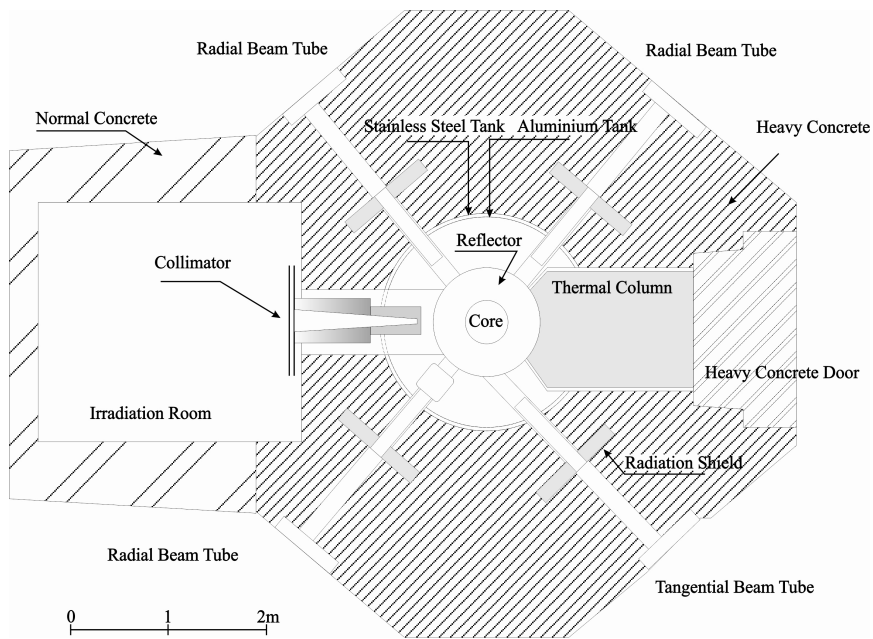


Figure 3.2: horizontal cross-section of the TRIGA Mark II reactor in Vienna

### 3.3 Reactor Core

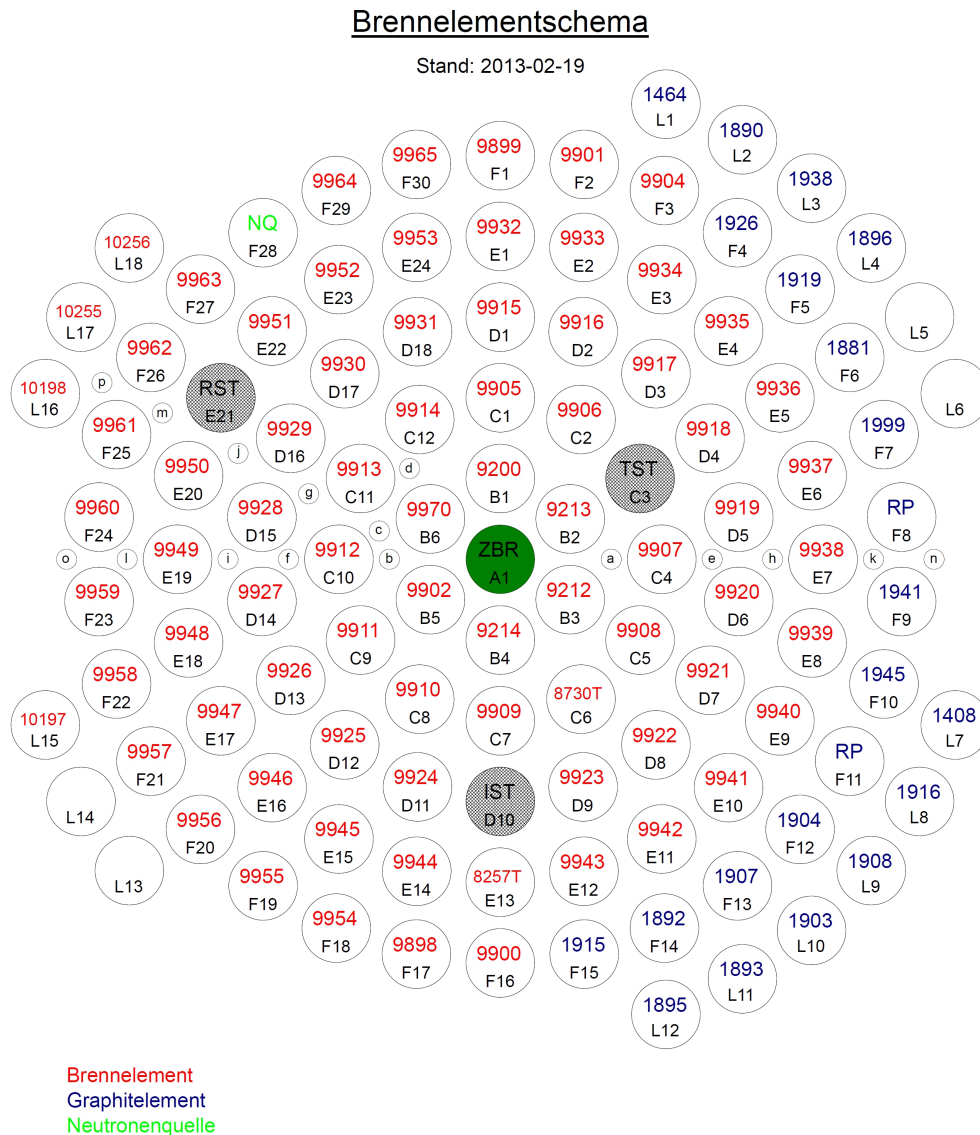


Figure 3.3: Reactor core setting on February 19<sup>th</sup> 2013. Fuel elements are marked red and graphite dummy elements are marked black.

Figure 3.3 displays a map of a reactor core setting in 2013. The reactor core consists of 90 core elements in an annular lattice structure, surrounding the central irradiation tube (*ZBR*). Inside the central irradiation tube samples are facing a thermal flux of  $1 \times 10^{13} \text{ cm}^{-2} \text{ s}^{-1}$ . [5] Emanating from the center, five rings (*B, C, D, E, F*) can be distinguished according to their radial distance to the *ZBR* in position *A1*. Regarding the core configuration in figure 3.3 the rings hold 72 fuel elements, 10 graphite dummy elements and three control rods (*RST, TST, IST*). The two fuel elements in positions *C6* and *E13* are equipped with thermocouples in the fuel meat, that allow to measure the

fuel temperature during reactor operation. A Sb-Be photoneutron source serves as a start-up source and continuously emits  $6 \times 10^6$  neutrons per second.[4] The core is held in association by two aluminum grip plates on the top and at the bottom of the core, with ninety-one holes for the core elements. Additionally to the ZBR there are sixteen further irradiation holes, where small samples can be inserted.[5]

### 3.3.1 Fuel elements

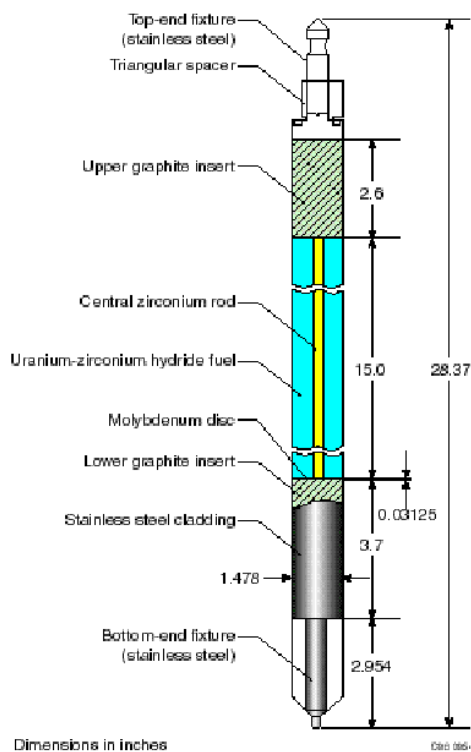


Figure 3.4: Fuel element of the TRIGA Mark II reactor.

The fuel elements consist of several components. The core of an element is a zirconium rod in the center. It is surrounded cylindrically along its whole length of 38,1 cm by the fuel meat, which is a homogenous mixture of 8 wt% uranium, 1 wt% hydrogen and 91 wt% zirconium. Figure 3.4 shows a fuel element of the TRIGA Mark II reactor.

The enrichment of the Uranium is 19,8% and therefore LEU. As mentioned above the zirconium hydride serves as the main moderator. The fact that its moderating abilities are temperature dependent and that it has a very strong negative temperature coefficient of reactivity, enables reactor operation in pulse mode (see chapter 3.1).[5]

Besides that, UZrH is convincing in terms of good heat capacity and low reactivity with water.

Below the fuel meat there is a molybdenum disc, which is a burnable poison, and on top and at the bottom of the fuel element there is a graphite element.[5] The cylindrical fuel is coated with a cladding of stainless steel or aluminum. The total length of a fuel element accounts for 72,24 cm and its diameter for 3,75 cm.

### 3.3.2 Irradiation history of the fuel elements

Since the start of operation in 1962 the Vienna TRIGA reactor had been using a mixed core consisting of aluminum clad (Al) and stainless steel (SST) clad low-enriched uranium (LEU) fuel and a few SST high-enriched uranium (HEU) fuel elements. Within the scope of the US Spent Fuel Return Program, the Technische Universität Wien/ATI returned those 9 HEU fuel elements to the United States. Furthermore most of the remaining LEU fuel elements were close to reaching their maximum burnup and Austria represents the position not to store any spent nuclear fuel on its territory. In 2011 negotiations started between the involved Austrian ministries, the US Department of Energy (DOE) and the International Atomic Energy Agency (IAEA). The parties' aims where to find solutions concerning the return of the spent HEU and LEU fuel elements and to possibly enable the operation of the reactor for the next decades. The achieved agreement suggested that Austria will return 91 spent fuel elements to the Idaho National Laboratory (INL) while INL offers 77 very low burnt SST clad LEU elements for further operation. The fuel exchange was performed successfully and at the end of October 2012 the new core arrived at the TRIGA Mark II reactor Vienna. On November 7<sup>th</sup> the reactor reached criticality using 64 fuel elements.[6]

75 of the 77 very low burnt fuel elements had been used in the Musashi reactor in Japan in the 1980ies. Their burn-up was less than one percent. The two remaining fuel elements came from Cornell University and had a burnup slightly above 1%. After further testing the reactor went back to normal operation in January 2013. Its core load consisted of 71 low-burnup fuel elements and five fresh fuel elements, which had been stored at the ATI.[3]

After the production was moved from General Atomics in the US in the nineties, the production of all types of TRIGA fuels are now subject to CERCA in France. Currently there is no production at all, because the authorities are working on implementing new post-Fukushima safety improvements into the fuel.

### 3.3.3 Control Rods

The reactor is controlled by three control rods, which contain powdered boron carbide ( $B_4C$ ) as absorber material. The rods are 40cm long and covered by an aluminum cladding. When they are fully inserted into the reactor core they absorb the neutrons continuously emitted from a start-up source and the reactor remains sub-critical. If the absorber rods are withdrawn from the core the number of fissions in the core and the power level increases.[4]

The control rod closest to the center of the reactor core is located in position C3 and called *Shim Rod (TST)*. Its diameter is 3,2 cm and it has a strong impact on the central neutron flux. At position D10 there is the *Safety or Transient Rod (IST)* that has 2,5 cm of diameter. While the other two control rods are withdrawn from the core by an electric motor, the transient rod can be moved pneumatically. The rod with the narrowest diameter of 2,2 cm and the biggest radial distance from the center is the *Regulating Rod (RST)* is set in position E21.[7]

Properties	Shim Rod (TST)	Transient Rod (IST)	Regulating Rod (RST)
Length [cm]	40	40	40
Diameter [cm]	3,2	2,5	2,2
Position	C3	D10	E21

Table 3.1: Properties of the control rods.

The reactor can be shut down either manually or automatically by the safety system. It takes about 1/10 of a second for the control rods to fall into the core.[4]

### 3.3.4 Graphite dummy elements

Additional to fuel elements there are as well reflector elements in the core. Those so-called dummies appear identical to the actual fuel elements, but consist of nuclear grade graphite and an aluminum cladding around them. Even though the graphite elements are not made of fissile material, their reflecting properties lead to an increase in reactivity by 10 c per dummy element inserted.[7]

### 3.3.5 Reactor Instrumentation

The I&C system of the reactor was renewed four times during the operation history of the TRIGA Vienna. The last replacement took place in 2015, where the old digital software based system by GA was exchanged with a generation 4-digital system by Škoda Company. Following the existing concepts, the whole system consists of SCRAM logic, neutron flux measurement channels (Operational Power Measurement *OPM*, Independent Power Measurement *IPM*, Pulse Power Measurement *PPM*), neutron detectors (fission wide-range chamber, compensated ionization chambers, non-compensated ionization chamber), I&C field instrumentation, a control system, a new operator's console and data acquisition system.[1]

### References Chapter 3

- [1] Villa, M., Bergmann, R., Kroc, M., Prokš, M., Valenta, V., Kaše, M., Herrmann, J., Matoušek, J., Böck, H.: The new I&C system of the TRIGA Mark II reactor Vienna, Wien 2015
- [2] Böck, H., Villa, M.: The TRIGA Reactor Vienna within the World of TRIGA-Research Reactors, Wien 2016
- [3] Herzog, H.: "Development and Validation of a Serpent-2 model for the TRIGA Mark II reactor of the Technical University Vienna"/Master Thesis, Universität Wien 2017
- [4] Sicherheitsbericht für das Atominstitut der Österr. Universitäten, Vienna University of Technology Dezember 2006, AIAU 26314
- [5] General Atomic (GA): TRIGA Mark II Reactor General Specifications and Description. General Atomic Company, U.S.A. March 1964
- [6] Villa, M., Bergmann, R., Musilek, A., Sterba, J., Böck, H., The Core Conversion of the TRIGA Reactor Vienna, Vienna University of Technology
- [7] Böck, H., Villa, M.: Praktische Übungen am Reaktor, Vienna University of Technology 2005, AIAU 25315

## 4.

### **Serpent –**

## **A Continuous-energy Monte Carlo Reactor Physics Burnup Calculation Code**

Simulation codes have been the tool of choice for modelling reactor geometries and predicting interaction physics in nuclear processes for many years. The state of the art is using the continuous-energy Monte Carlo method to perform criticality safety analyses, radiation shielding and dose rate calculations, detector modelling and the validation of deterministic transport codes.[1]

Serpent is a multi-purpose three-dimensional continuous-energy Monte Carlo particle transport code, developed at VTT Technical Research Centre of Finland, Ltd.[2] The team started writing the code in 2004 and it was first publically available in 2009 via OECD/NEA Data Bank and RSICC. Currently the version Serpent 2 finds itself in the testing state with its capabilities extending beyond reactor modelling. The applications can be roughly divided into three categories: [2]

- Traditional reactor physics applications, including spatial homogenization, criticality calculations, fuel cycle studies, research reactor modelling, validation of deterministic transport codes, etc.;
- Multi-physics simulations, i.e. coupled calculations with thermal hydraulics, CFD and fuel performance codes;
- Neutron and photon transport simulations for radiation dose rate calculations, shielding, fusion research and medical physics;

In this thesis Serpent is mainly used to calculate the k-eigenvalue of configurations and to perform burn-up calculations.

## 4.1 Geometry Input

To reflect the behaviour of the real fuel element configuration and reactor as closely as possible, a 3D-modell has to be developed in Serpent. This happens in similarity to Monte Carlo Neutron Physics (MCNP) and other nuclear physics codes, using a universe-based constructive solid geometry (CSG). That means, that that the geometry is divided into separate levels, which are all constructed independently and nested one inside the other. [3] This enables to break down a complex geometry into smaller parts. The very basic elements of the geometry are the homogenous material cells that are defined by their filling material and the surface types. Serpent supports regular geometry structures, like square and hexagonal lattices, but also special geometry types.[2]

## 4.2 Neutron Population and Criticality Cycles

Once the geometry is completed, certain simulation parameters must be set, including reactor power and output options.

The default calculation mode is the  $k$ -eigenvalue criticality source method. It is run in cycles and the source distribution of each cycle is formed by the fission reaction distribution of the previous cycle.[3] The first cycle starts at  $k_{eff} = 1$  and approaches its real source size by increasing or decreasing  $k_{eff}$  in every cycle. The number of source neutrons per cycles (<npop>), active cycles run (<cycles>) and inactive cycles run (<skip>) have to be defined by the user first. Inactive cycles help to find a more precise initial fission source distribution, before actually collecting results in the active cycles.[3] The input parameters have to be set in the following order:

```
set pop <npop> <cycles> <skip>
```

The values for these parameters stayed the same throughout all simulations done for this thesis:

```
set pop <1000000> <1500> <70>
```

In case of all fissile material being located in a region that is small compared to the geometry dimensions, the initial source sampling can be skipped by switching to

external source mode. This second mode allows the user to define an external source, which emits all starting neutrons.[3; 4]

### 4.3 Particle tracking

For performing its neutron transport calculations Serpent benefits from a combination of the surface-tracking and Woodcock delta-tracking method. In the scope of the transport algorithm, particles are chased through the geometric configuration from their incidence to their eventual absorption or escape of the geometry.[5] The overall interaction probability of a particle along the distance of one cm is given by the macroscopic cross section of a material  $\Sigma$ . As described in equation (2.6),  $\Sigma$  also equals the reciprocal of the mean free path length. Just like the particle, the transport simulation follows a random walk in between interaction events. The procedure includes sampling the free path length till the next collision point, transporting the neutron there and assuming an interaction. In case that the interaction is scattering, the procedure starts all over with updated direction and particle energies by estimating the distance to the next collision.[5] The Monte Carlo simulation creates and processes the history of millions of particles.

*Surface-tracking* is the standard transport calculation method for Monte Carlo simulations. The notion behind that method is based on the fact that any point of the path can be considered the starting point of a new path.[5] That means that the track of the sample path can be stopped, when the particle crosses the boundaries of two different materials. Afterwards the next path length can be sampled by using the macroscopic cross section of the new material.[5]

The second option for particle tracking is the *Woodcock delta-tracking* method. Instead of stopping and recalculating with the new material cross section at every boundary, this method is based on the concept of virtual collision.

Virtual collisions are fictive interactions that have no impact on the statistics of the random walk and preserve the energy ( $E$ ) and direction ( $r$ ) of the particle.[5] This means, that the virtual collision cross section  $\Sigma_0$  does not affect the simulation and that the material cross section  $\Sigma$  can be adjusted to a cross section  $\Sigma'$  defined as:

$$\Sigma'(r, E) = \Sigma(r, E) + \Sigma_0(r, E) \quad (4.1)$$

Using different virtual cross sections allows to modify the regions of different material (1, 2, 3,..) in a way that their majorant cross section  $\Sigma_m$  stays the same.  $\Sigma_m$  represents the maximum of all material totals at each energy point and is independent of spatial coordinates.[5]

$$\Sigma'_1(E) = \Sigma'_2(E) = \Sigma'_3(E) = \dots = \Sigma_m(E) \quad (4.2)$$

The thus gained uniform macroscopic cross section can be used for sampling path length that keep their validity throughout the geometry and regardless of material boundaries crossed. If the collision at the end of the path is either real or virtual, depends on the ratio  $P$  of the physical total cross section to the majorant cross section.

$$P = \frac{\Sigma(r, E)}{\Sigma_m(E)} \quad (4.3)$$

In case of a virtual interaction the procedure starts over until a real collision is detected.[4]

#### 4.4 Burnup calculation

When run as a stand-alone burnup calculation Code, Serpent can perform a burnup routine by solving the Bateman equations. Those equations describe the changes in the material compositions, caused by neutron induced reactions and radioactive decay.[3]

That requires several additional inputs, covering the identification of the depleted materials and information concerning the irradiation history. The information about burnup and the irradiation history can be set up in units of time in days or burnup in  $MWd/kgU$ . [2] Further parameters allow to divide burnable material into any number of depletion zones, which gives more precise burnup results for the considered region.

After processing the input, Serpent chooses the fission and activation products and the actinide daughter nuclides for the calculation. For simple geometries the code calculates as well the masses and volumes needed. Reaction rates are normalized to total power, specific power density, flux, fission or source rate.[2]

Serpent features two approaches to solve the Bateman equation introduced above:

- Transmutation Trajectory Analysis method (TTA)
- Chebyshev Rational Approximation method (CRAM)

The first TTA routine is based on the analytical solution of linearized depletion chains, while CRAM is an advanced matrix exponential solution developed for Serpent at VTT.[2]

During its transportation routine Serpent calculates the flux-volume-averaged one-group transmutation cross sections. To speed up these calculations Serpent uses the spectrum collapse method. This method includes collapsing the continuous-energy reaction cross sections after the calculation has been completed, using a collected flux spectrum.[2]

#### **4.4.1 Output files and Burnup results**

The data output is collected into files after each burnup step of the calculation. The main Matlab output file for each Serpent simulation contains all results that were calculated by default during the transport cycle. It is called `<input>_res.m`, where `<input>` is the user defined name of the input file. Among further data it provides run and delta-tracking parameters, run statistics, energy grid, nuclides and reaction channels and parameters for the burnup calculation.[3]

The output of the burnup calculation in independent calculation mode is collected into a Matlab file called `<input>_dep.m`. It lists the number of burnup steps, inventory nuclides and material parameters for the depleted material, especially the activities, spontaneous fission rates and decay heat data. An additional option is to write the new

material composition after every step of the burnup calculation into a separate output file named `<input>_bumat<n>`, where `<n>` refers to the respective burnup step.[3]

For this thesis the most important information from the output files include the multiplication factor  $k$ , total power, information on the calculation process, radioactivity data and further criticality eigenvalues. Another major tool for calculating the fuel time evolution was processing the data from the updated fuel composition files after the burnup intervals.

## 4.5 Data Libraries

Serpent processes continuous-energy cross sections from ACE format data libraries and uses classical collision kinematics for any interaction. The data banks covered within the Serpent installation package are JEF-2.2, JEFF-3.1, JEFF-3.1.1, ENDF/B-VI.8 and ENDFB/B-VII. Proper interaction data is available for 432 nuclides at six temperatures between 300K and 1800K and the libraries host decay data for almost 4000 nuclides and meta-stable states.[2]

Serpent does not use the continuous energy cross sections directly from the libraries, but first reconstructs a master energy grid and then starts the neutron transportation simulation.[4] In a similar manner the macroscopic cross sections for materials are pre-calculated before the start of the transport routine to make the latter crucially faster.

In order to adjust the temperatures of ACE format cross sections, a Doppler-broadening pre-processor routine is implemented. This allows to describe the actual interaction physics more precisely in temperature-sensitive applications.[2]

## 4.6 Running Serpent

The very start of running Serpent in  $k$ -eigenvalue criticality source mode is initialized by the user's input. It provides information about the geometry of the given fuel element and reactor configuration and defines the composition of the present materials according to chapter 4.7. Furthermore the user can choose between different options for running the calculations and the used libraries. After acquiring the necessary cross

sections and data from a library, Serpent processes the input and shares the gathered data.[4]

Subsequently Serpent starts with its main particle transportation cycle. Thanks to thread-based OpenMP and distributed-memory MPI parallelization, Serpent can be run in parallel in multi-core workstations. That means that the particle transport simulation, can be split up between several CPUs.[2] It is the same case for performing a burnup simulation, where the pre-processing and depletion routines can be divided as well.

When the calculation is finished, the gathered results are written into the described output data files that are open to the user.

According to the user's demands Serpent can create several geometry plots in all planes. Additional to that Serpent has a built-in capability to visualize the neutronics in thermal systems by plotting the fission power and thermal flux distributions into a graphics file.[3]

## 4.7 Implementation of the Serpent Reactor Model

All the following calculations in the thesis are executed using a pre-validated three-dimensional simulation model of the TRIGA Mark II Vienna, developed by the means of Serpent. The code of any Serpent simulation can be roughly subdivided into the main geometrical input, consisting of cells, surfaces and material definitions, plotting parameters and output parameters.

### 4.7.1 Geometry

The three-dimensional Serpent reactor model was reproduced using the geometry and material data from an already evaluated MCNP model. This model considers all components of the reactor construction and the actual reactor core in the chapters 3.2 and 3.3. Even though some non neutron-impacting simplifications already assumed in the MCNP model were adapted into Serpent as well, the reactor model gives a precise base for any neutron transportation calculations.[6]

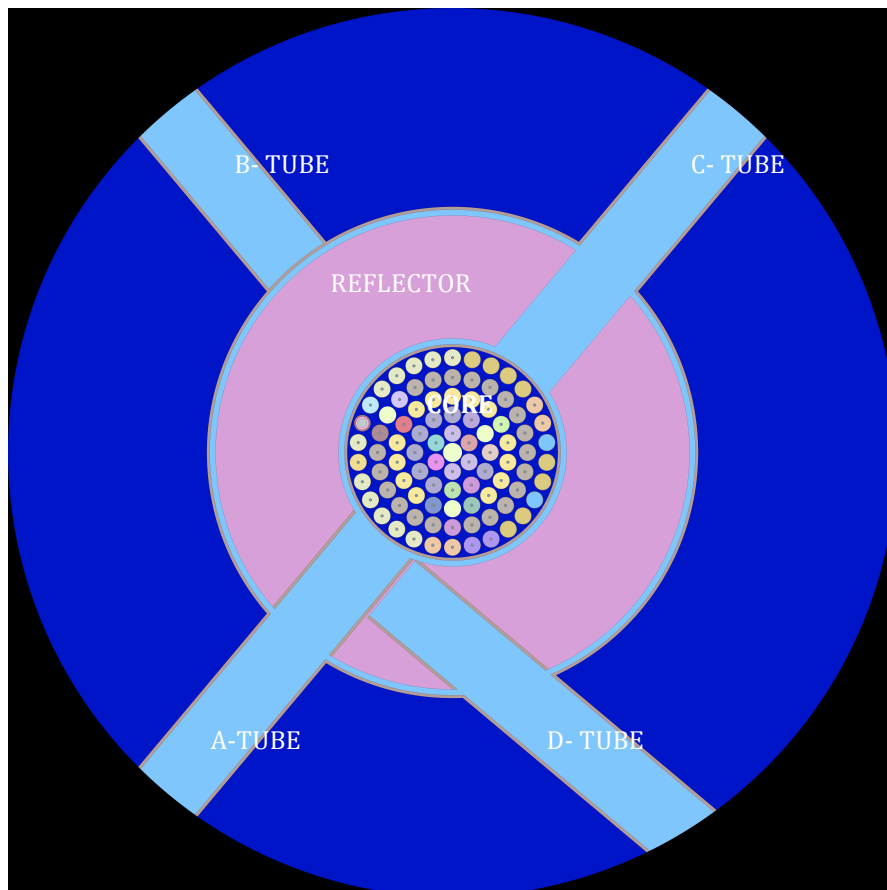


Figure 4.1: Horizontal view of the Serpent reactor model at  $z=-9.65$  cm.

Figure 4.1 presents a horizontal view of the Serpent reactor model below the middle of the reactor at  $z=-9,65$  cm. It depicts the reactor core, its annular groove graphite reflector and the beam tubes inside the cylindrical water tank, which has a radius of 100 cm and a total height of 120 cm.[4] The different colours in the plot represent different materials. Especially in the core the varying amounts of uranium-235 in the fuel elements and the graphite dummy elements are visible. The empty positions of the control rods that are fully extracted in this plot and the central irradiation tube are filled with water.

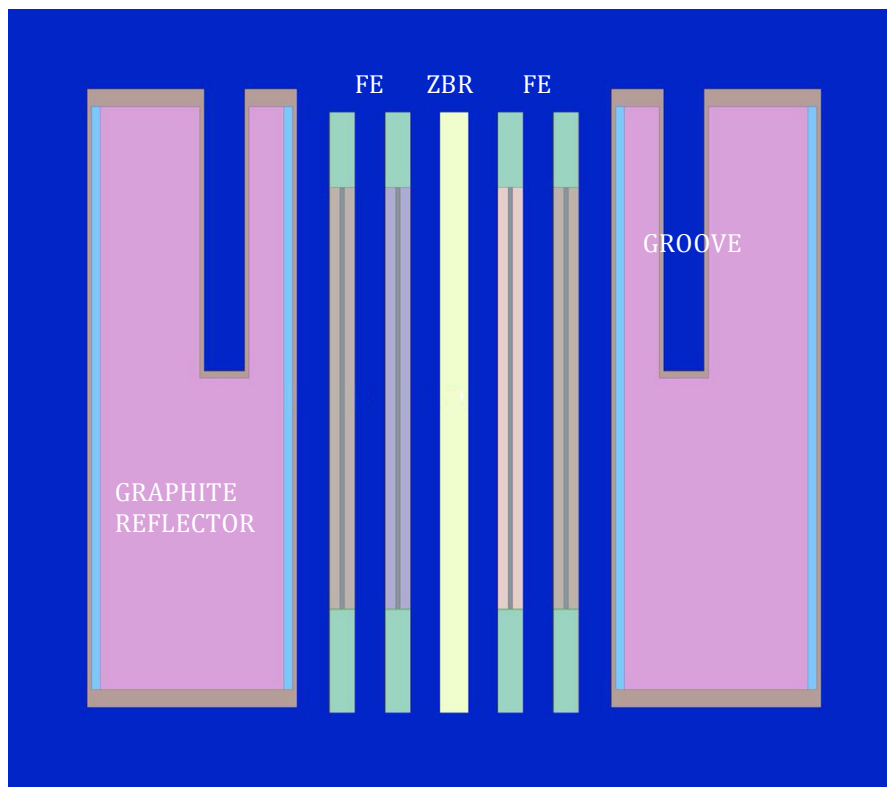


Figure 4.2: Vertical view of the Serpent reactor model at  $y=0$  cm.

Figure 4.2 provides a vertical view of the reactor model at  $y=0$  cm and shows the cross sections of the central irradiation tube (ZBR), some fuel elements and the groove graphite reflector.

The centre of the fuel elements (FE) in figure 4.2 consists of a cylindrical zirconium rod that is coated by the fuel meat. As mentioned above, the fuel meat composition is different for three of the four presented fuel elements. On top of the fuel meat of each fuel element there is a graphite reflector and below the fuel meat there is a molybdenum-disk and another graphite reflector.[7]

#### 4.7.1.1 Surface and Cell Cards

Surface cards are needed to specify the geometry of the modelled component and to define the borders of the cells. Serpent already provides the most common and elementary surface types, i.e. cylinder, sphere and plain surfaces. The syntax of the surface card is:

```
surf <id> <type> <param 1> <param 2> ...
```

<id> represents the arbitrarily chosen surface identification number, which helps to identify the surfaces in the cell definitions. <type> refers to the geometry of the surface and <param 1> <param 2> ... are called surface parameter. Accordingly to the surface type the coordinates either set the distance from the core centre or define the coordinates of the surface centre and the radii.[3]

The cells are the basic building blocks of the geometry. Their boundaries are defined by surfaces and the space in the cell is either filled with a homogenous material, another universe or void. The cell-defining syntax is:

```
cell <name> <u0> <mat> <surf 1> <surf 2> ...
```

The identification number of the cell is represented by <name>, followed by the universe number of the cell <u0> and the material composition that fills the cell <mat>. <surf 1> <surf 2> ... determine the boundaries of the cell. Every cell belongs to a universe, which is defined by the user-input for cell universe number and allows dividing the geometry into separate levels. The different universes can as well be nested into each other. In that case the very outside universe should be labeled as number 0.

#### 4.7.1.2 Universes and lattice-based structure

All core elements, i.e. the fuel and dummy elements, control rods, the neutron source and the irradiation tubes, are defined by the joint universe number of their cells. For example, universe number 10 represents fresh fuel elements and universe number 18 the shim rod. They were initially modelled separately from each other with their origins at x=0 cm and y=0 cm each.

In a second step the core elements were put in their right places in the core model by implementing the respective universe number in the right position in the annular core lattice.

The core of the TRIGA Mark II reactor Vienna is arranged in a circular cluster array, for which Serpent already offers a pre-defined lattice. Lattices are special universes, filled with the regular structure of other universes, for example the fuel pins, dummy graphite elements or the control rods.[3] The syntax for a circular cluster array is:

```
lat <u0> <type> <x0> <y0> <nr>
```

where the command `lat` introduces a lattice structure. `<u0>` defines the universe number of the lattice and `<type>` the pre-implemented type of lattice. In case of a circular cluster array the lattice type is number 4. `<x0>` and `<y0>` refer to the x and y coordinate of the lattice origins and `<nr>` is the number of rings in the array.[3] The syntax for the TRIGA Mark II core looks as follows:

```
lat 100 4 0 0 6
```

The rings `<nr>` in the lattice are defined by:

```
<n> <r> <theta> <u1> <u2> ... <un>
```

With `<n>` holding the numbers of sectors in the ring and `<r>` giving the central radius of the ring. `<theta>` is the angle of rotation and `<u1>` `<u2>` ... `<un>` are the universes filling the sectors.[3] The TRIGA Mark II reactor core consists of 6 rings. The inner ring called *A* holds just one core element (`<n>=1`) and has a radius of 0 cm (`<r>=0.0`). The *A*-ring is surrounded by the *B*-ring, which covers 6 core elements (`<n>=6`) and has a radius of 4,145 cm (`<r>=4.145`). The syntaxes for the remaining rings *C*, *D*, *E* and *F* are analogue to the first two rings. In order to reproduce the MCNP model, the single rings have to be rotated by 30° (`<theta>=30`).

The spaces in between the core elements and around the core are fully covered with water in the model. Eventually the lattice with universe number 100 is continually occupied by universe numbers of the single core elements and the water.[4]

The graphite reflector was modelled separately from the core. It is coated by aluminum with an air gap in between the graphite and the cladding. As shown in figure 4.2 the

upper half of the reflector is interrupted by an annular groove for irradiation experiments. To restrain the cells of the reflector from overlapping and any further errors by Serpent, the geometry was divided into four several universes.[4]

Further components of the reflector are the beam tubes reaching through both the reflector and the water tank, as seen in figure 4.1. The tubes were again modeled separately and then inserted into the correct reflector universe.

After that the core and the reflector, including parts of beam tubes, are positioned into the cylindrical water tank, which is the outermost universe and label as number 0. The tank is filled with the reactor core, the reflector and the remaining parts of the beam tubes, passing through the tank.[4]

#### 4.7.1.3 Material Definitions

The homogenous materials filling the cells of the geometry are defined using material cards. Each material consists of numerous nuclides and each nuclide is connected to a cross section library, as commanded in the input file.[3] The calculations in this thesis were performed using ENDF/B-VII.

The syntax to list nuclides in Serpent is:

```
<Z><A>.<id>
```

where <Z> is the atomic number of the nuclide, <A> is the isotope mass number and the library id <id> refers to data evaluation or temperature. The syntax for a material card looks like this:

```
mat <name> <dens>
<iso 1> <frac 1>
<iso 2> <frac 2>
...
```

The card determines the name <name> and either the atomic or the mass density <dens> of the material in units of  $10^{24}/\text{cm}^3$  or  $\text{g}/\text{cm}^3$ . <iso 1>, <iso 2> ... list the constituent nuclides and <frac 1>, <frac 2> ... their corresponding mass or atomic fractions.[3] For instance the material card representing the Transient rod consists of boron-10, boron-11 and natural carbon:

```
mat fillCR -2.48  
5010.03c -0.14925  
5011.03c -0.60075  
6000.03c -0.25
```

Further examples for material cards are give in table 5.1 and table 6.3.

Regarding moderating material like hydrogen, carbon or zirconium hydride thermal scattering cards are introduced. Those cards are implemented into the material cards and replace the free-atom cross sections by thermal scattering cross sections. Thermal cross sections take the thermal properties of the moderating material into account and therefore prevent significant errors in the spectrum and results of modeled thermal systems. The library used for thermal scattering data is the MCNP6 library.[3]

Simulation and output parameters were chosen accordingly to chapter 4.2 and 4.6.

## References Chapter 4

- [1] Serpent, URL: <http://montecarlo.vtt.fi/development.htm>  
[Date: 2018-08-14]
  
- [2] Serpent, URL: <http://montecarlo.vtt.fi>  
[Date: 2018-08-14]
  
- [3] Leppänen, J.: Serpent – a Continuous-energy Monte Carlo Reactor Physics Burnup Calculation Code. User’s Manual, 2015
  
- [4] Herzog, H.: “Development and Validation of a Serpent-2 model for the TRIGA Mark II reactor of the Technical University Vienna”/Master Thesis, Universität Wien 2017
  
- [5] Serpent, URL: [http://serpent.vtt.fi/mediawiki/index.php/Delta-\\_and\\_surface-tracking](http://serpent.vtt.fi/mediawiki/index.php/Delta-_and_surface-tracking)  
[Date 2018-08-17]
  
- [6] Cagnazzo, M.: “Neutronic modelling of the new TRIGA core and experimental validation”/Dissertation, Vienna University of Technology 2018
  
- [7] General Atomic (GA), March 1964, TRIGA Mark II Reactor General Specifications and Description. General Atomic Company, U.S.A.

**Simulations**

**&**

**Discussion of the Results**

## 5.

### Core I,

#### 2013-01-21 to 2013-07-22

After the major fuel element exchange in October 2012, the core configuration “Core I”, started critical operation on January 21<sup>st</sup> 2013. The configuration consisted of 72 fuel elements (*FE*) and 10 dummy elements and is presented in figure 3.3. Core I was in operation until July 2013.

#### 5.1 Update of the fuel element configuration

The configuration “Core I” was composed of several fresh fuel elements (9200, 9212, 9213 and 9214) and for its majority of fuel elements that were already irradiated before, as described in chapter 3.3.2. The previously irradiated presented an initial, even if very low burnup value. In order to simplify their reproduction in the Serpent input file, the fuel elements were hence categorized into several burnup groups (1%, 0,85%, 0,75%, 0,62% or 0,54%) and fuel elements belonging to a certain burnup group were described uniformly in Serpent. Table 5.1 displays the various fuel compositions for fresh fuel and fuel with a burnup of 0,85%, 0,75%, 0,62% or 0,54% and 1% in [ $g/cm^3$ ].

Elements	fresh FE	Used FE 1% Burnup	Used FE 0,85% Burnup
U-235	0,016566876	0,016401207	0,016426058
U-238	0,066774839	0,066774839	0,066774839
Zr-90	0,901187518	0,901187518	0,901187518
H-1	0,015470767	0,015470767	0,015470767
Elements	Used FE 0,75% Burnup	Used FE 0,62% Burnup	Used FE 0,54% Burnup
U-235	0,016442624	0,016464161	0,016477415
U-238	0,066774839	0,066774839	0,066774839
Zr-90	0,901187518	0,901187518	0,901187518
H-1	0,015470767	0,015470767	0,015470767

Table 5.1: Fuel element composition for the various levels of burnup all given in [ $g/cm^3$ ]

Once the composition of each element is adjusted in the simulation, they have to be put in their actual position in each ring. The whole core configuration is shown in figure 5.1. Elements of the same colour consist of the same fuel composition or material. The blue colour represents water in all horizontal plots. Serpent chooses the rest of the colours in the plot randomly.

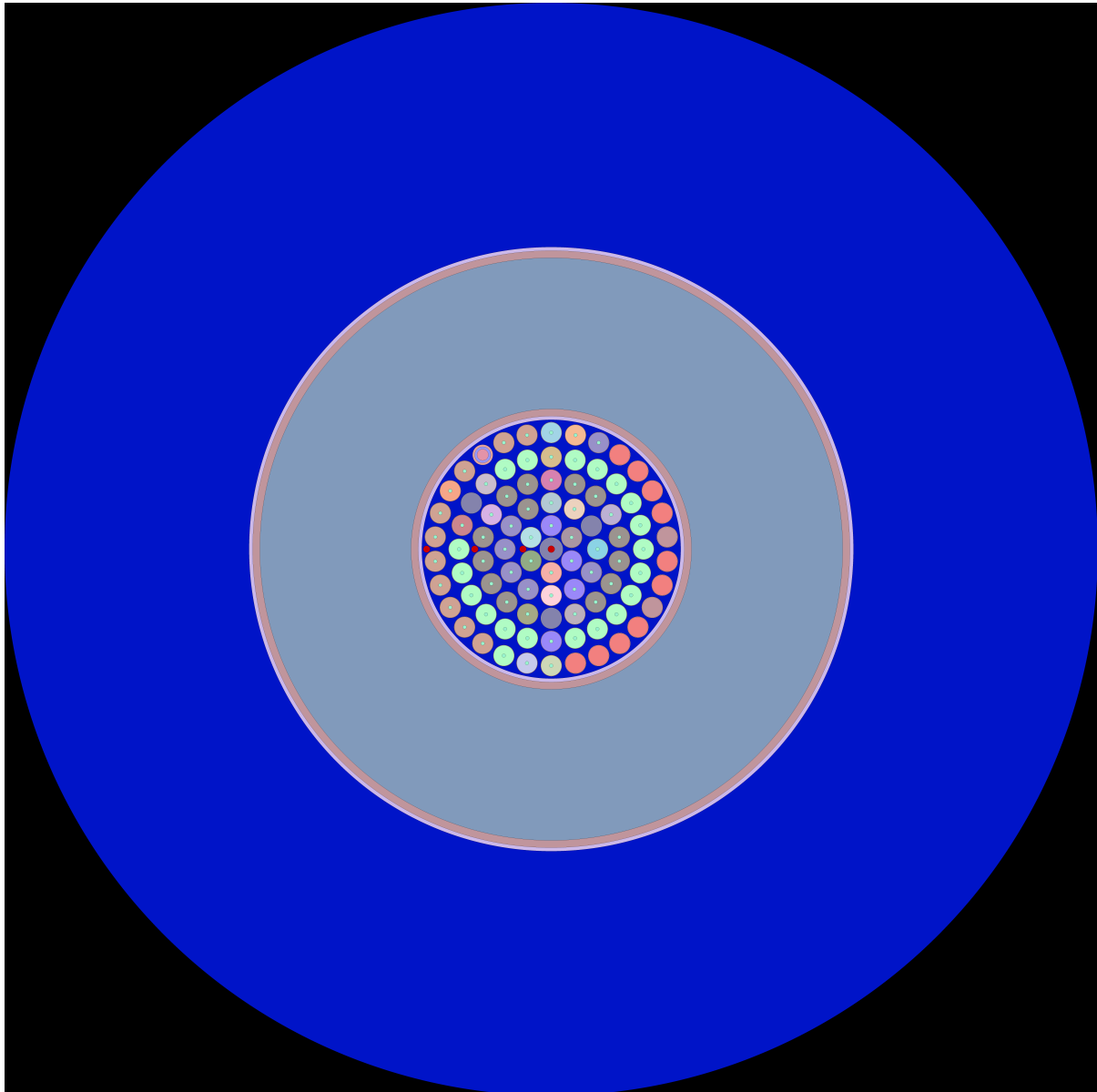


Figure 5.1: Top view of the TRIGA Mark II core configuration on January 21<sup>st</sup> 2013

To keep the calculation effort and time manageable, 20 representative fuel elements were picked to calculate the fuel time evolution. There was at least one representative for each burnup group in each ring, plus all the elements in the positions around the control rods. As the rings are placed in a concentric arrangement around the ZBR, it was

decided to adapt the calculation results of the representative elements to the elements in the ring. The mentioned time evolution of the fuel elements will be discussed in chapter 5.4.

## 5.2 Modelling of the Control Rods

After updating and recreating the fuel element configuration the three control rods are introduced into the system at positions C3 (Shim rod), D10 (Transient rod) and E21 (Regulating rod). Their active length is 38,1 cm and equal to the active length of the fuel elements, while the diameter is different for each rod. The structure of the control rods is the same and composed of an absorbing cylindrical body made of boron carbide ( $B_4C$ ) that is covered by an aluminum cladding. The absorber material  $B_4C$  consists 75% of boron-10 and boron-11 and 25% of naturally occurring carbon and has a density of 2,48 g/cm<sup>3</sup>.

Properties	Shim Rod	Transient Rod	Regulating Rod
Active Length [cm]	38,1	38,1	38,1
Diameter [cm]	1,60	1,25	1,10
Diameter [cm] incl. Al-cladding	1,6711	1,3210	1,1711
Composition	$B_4C$	$B_4C$	$B_4C$
Position	C3	D10	E21

Table 5.2: Further information about the structure of the control rods

$B_4C$	[g/cm <sup>3</sup> ]
B-10	0,14925
B-11	0,60075
C	0,25

Table 5.3: Composition of  $B_4C$

### 5.2.1 Worth of the Control Rods

Each rod can be attributed with a reactivity value in Dollar, called the worth of the rod.[1] This refers to the maximum amount of reactivity that can be inserted into the system by pulling the respective control rod completely out of the core and is connected to the rod's ability to absorb neutrons.

To ensure the accuracy of the reactor model in the Serpent simulation, results for calculating the rod worth of the control rods should be as close as possible to the experimental data.

### 5.2.2 Experimental calibration of a Control Rod

The measurement routine is explained by the example of determining the calibration curve of the regulating rod. The process is analog for the shim and the transient rod.

As starting condition the transient rod is fully extracted from the core and the regulating rod is fully inserted in the core. The shim rod gets partially extracted until the reactor power reaches criticality at 10 W. Then the regulating rod is removed step-by-step and the reactor period is determined by the stopwatch method.[1] The averaged stopwatch time can be converted into the reactor period  $T$  using equation (2.18) and the corresponding reactivity is given by the inhour equation or the inhour diagram. After the first step the regulating rod remains in its new position and the shim rod is moved down until the reactor is back at criticality at 10 W. This procedure has to be repeated until the regulating rod is fully extracted from the core.[1]

The gained reactivity values can now be assigned to the respective rod position, which creates the rod calibration curve. The integral calibration curve equals the worth of the control rod. This is illustrated in figure 5.3.

The expected results for the total control rod worth depend on their radial distance from the center of the reactor core and their geometrical structure. The closer the control rod is to the center and the larger its diameter, the stronger is its impact on the core and the bigger is the worth of the rod. Therefore the highest reactivity value belongs to the shim rod, followed by the transient rod and the regulating rod, which holds the lowest reactivity value.

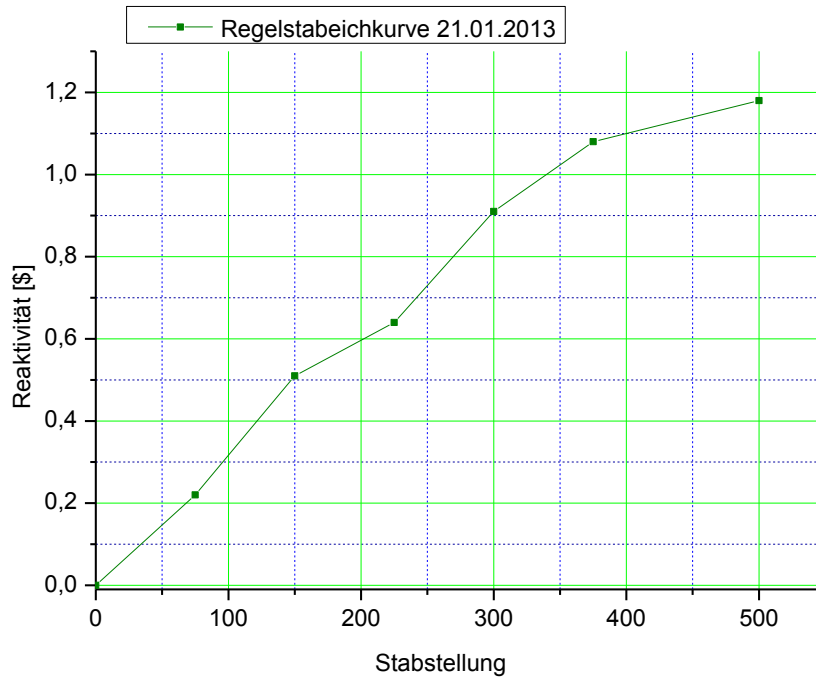


Figure 5.3: Calibration curve of the Regulating rod. The total rod worth adds up to 1,2 \$.

### 5.2.3 Simulation of the Control Rod Worth

The first step to evaluate the worth of the different control rods in the simulation is to run Serpent at  $k$ -eigenvalue criticality source mode, where all three rods are completely extracted from the core and their positions inside the core are filled with water. The thus calculated  $k_{eff}$  serves as the benchmark value and refers to the core in absence of all neutron absorbing and power-controlling elements. The expected result is  $k_{eff} > 1$ . Using equation (2.19)

$$\rho [PCM] = \frac{k-1}{k} \quad (2.19)$$

and the conversion factor

$$\rho [\$] = \frac{\rho [PCM]}{0,0073} \quad (5.1)$$

gives the reactivity value for the configuration in dollars. Due to the peculiarity of the research reactor  $\beta_{eff} = 0,73\%$  is used instead of  $\beta_{abs} = 0,64\%$ .

The second step requires rerunning the Serpent code, but differently to the first time, one control rod is fully inserted into the core and the other two are fully removed. The gained  $k_{eff}$  describes the state of the core configuration with one inserted absorber rod

and the reactivity left in the core. The conversion to dollars is analog to the first situation using (2.19) and (5.1).

The actual amount of reactivity that can be released when the analyzed control rod is fully withdrawn from the core, is the difference between situation one and situation two.

$$\Delta\rho_{Control\ rod} = \rho_{all\ rods\ out} - \rho_{one\ rod\ inserted} \quad (5.2)$$

This procedure has to be repeated for the remaining control rods, determining one after the other.

### 5.2.4 Comparison of Simulation and experimental Data

Table 5.4 shows the data of the rod worth simulations for the three control rods. The experimental results according to 5.2.2 are given in the blue colored *Experimental Rod value*-line. The last column shows the agreement of the simulation and the experimental measurement.

		All Rods extracted	Transient inserted	Regulating inserted	Shim inserted
<b>Serpent Simulation Output</b>	$k_{eff}$	1,019850	1,005990	1,009810	0,998059
	$\rho$ [PCM]	0,019464	0,005954	0,009715	
	$\rho$ [\$]	2,666253	0,815662	1,330781	
<b>Serpent Rod value</b>	$\Delta\rho_{Serpent}$ [PCM]		0,013509	0,009749	
	$\Delta\rho_{Serpent}$ [\$]		1,850591	1,335472	
<b>Experimental Rod value</b>	$\Delta\rho_{exp}$ [\$]		2,1	1,2	2,5
	$\Delta\rho_{exp}/\Delta\rho_{Serpent}$		113,48%	89,86%	

Table 5.4: Experimental and simulation results for the control rod worth. The  $B_4C$  density in the simulation is 2,48 g/cm<sup>3</sup>.

Comparing the results, the agreement between simulation and experiment lies within a quite large error range of 10 to 13%. The transient rod is worth more in the simulation than it is in reality, which means that it has a stronger impact on the reactivity when inserted in the simulation, than it actually has. The opposite applies for the regulating

rod. In case of the shim rod, the simulation does not reach criticality and no further conclusions can be drawn.

To start the simulation of the first core and the burnup as closely as possible to reality, the simulation values for neutron absorption have to be adjusted. This can be accomplished either by varying the geometrical structure or the density of the rods. The geometric measurements of the rods are predefined and have not changed during the operational years of the reactor. Therefore the most reasonable approach to obtain better results is to modify the density of each control rod. After trying several different densities the best agreement was found with 0,496 g/cm<sup>3</sup> for the regulating and 0,36 g/cm<sup>3</sup> for the shim rod. It was not necessary to change the density of the transient rod, because it remained completely extracted from the core during the conducted measurements. The results with the adjusted densities are given in table 5.5.

The new agreement of the core configuration simulation is good enough to execute additional simulations of other core parameters and determine the deviation of the simulation compared to the experimental results. The changed densities remain throughout all following experiments and core configurations and are no longer indicated in the tables.

		<b>All Rods extracted</b>	<b>Transient inserted</b>	<b>Regulating inserted</b>	<b>Shim inserted</b>
<b>Serpent Simulation Output</b>	$k_{\text{eff}}$	1,019850	1,005990	1,010830	1,001130
	$\rho$ [PCM]	0,019464	0,005954	0,010714	0,001129
	$\rho$ [\$]	2,666253	0,815662	1,467667	0,154620
<b>Serpent Rod value</b>	$\Delta\rho_{\text{Serpent}}$ [PCM]		0,013509	0,008750	0,018335
	$\Delta\rho_{\text{Serpent}}$ [\$]		1,850591	1,198586	2,511633
<b>Experimental Rod value</b>	$\Delta\rho_{\text{exp}}$ [\$]		2,1	1,2	2,5
	$\Delta\rho_{\text{exp}}/\Delta\rho_{\text{Serpent}}$		113,48%	100,12%	99,54%

Table 5.5: Experimental and simulation results for the control rod worth with changed B<sub>4</sub>C densities.

### 5.3 Core I Excess reactivity

The *core excess reactivity* is the amount of positive reactivity that can be introduced into the core by lifting the control rods into their final upper position, starting from the rod positions, where the core configuration had reached criticality.[2]

The excess reactivity has to be calculated for each respective control rod at a time. The sum of these excess reactivity values adds up to the total core excess reactivity.

$$\rho_{Core\ excess} = \rho_{excess\ Shim} + \rho_{excess\ Regulating} + \rho_{excess\ Transient} \quad (5.3)$$

The core excess reactivity is a crucial parameter in reactor safety for as long as  $\rho_{Core\ excess} < \beta$  the reactor cannot reach criticality with prompt neutrons only.

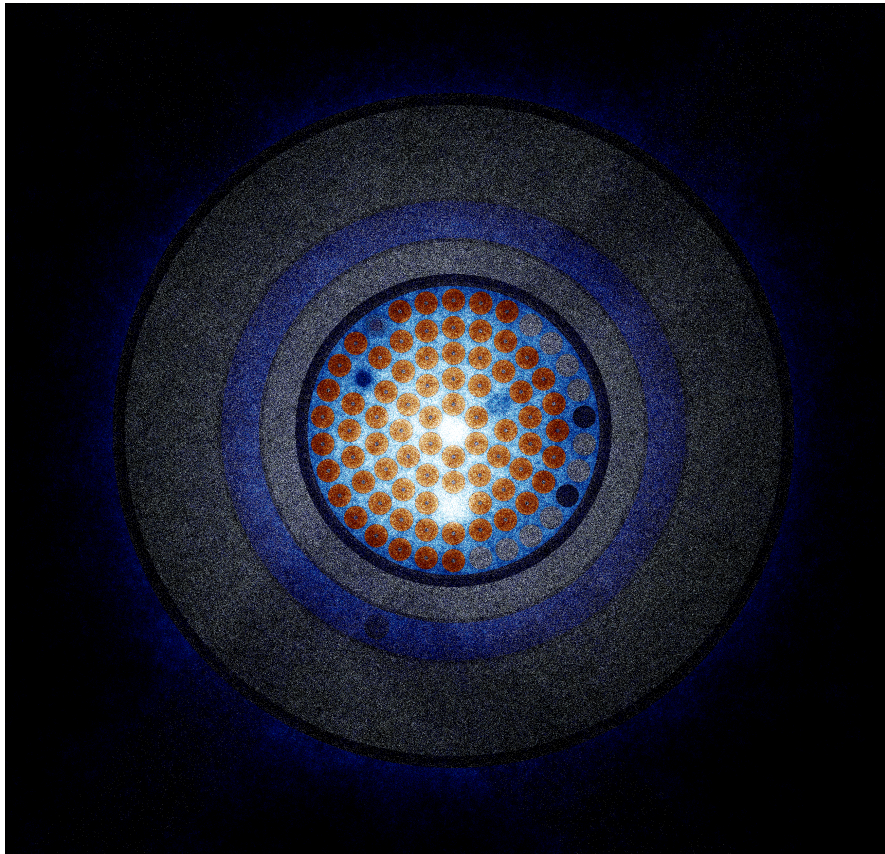


Figure 5.4: Plot of the fission power and thermal flux distributions of the core configuration for the core excess measurement with just 1000 Neutrons. The cold shades represent the relative thermal neutron flux. It peaks at the ZBR and the inner rings including the void space of the extracted Transient rod at D10. The two blue spots at positions C3 and E21 represent the partially inserted Shim and Regulating rod. The spot at E21 is darker because the Regulating rod is inserted more deeply at position 50 and absorbs more Neutrons than the Shim rod at the higher position 200.

### 5.3.1 Experimental determination of the Core Excess Reactivity

In order to bring the reactor up to a previously determined power level, the first step is to fully remove the transient rod from the core. In this experiment the selected power level is 10 W. The remaining shim and regulating rod are being partially extracted from the core until the reactor gets critical at 10 W. The I&C-system of the reactor displays the position of the control rods and the corresponding reactivity value can be taken from the reactivity calibration curves of the control rods.

The positions of the three rods relative to each other are not important in this experiment as long as the configuration is critical at the selected power level. The experiment was conducted using the configuration “Core I” on January 21<sup>st</sup> 2013. It is essential to perform this measurement on a Monday or after a longer period of time, where the reactor was not in operation. This insures that any decay products and produced reactor poisons with shorter half-lives have no influence on the experiment.

To calculate the excess reactivity of one rod, the reactivity connected to the rod position at 10 W [β] has to be subtracted from the total worth of the control rod [β]. The core excess reactivity is the sum of the excess reactivity values of each rod. As the transient rod is completely pulled out, it doesn't have an impact on the calculation.

	<b>Rod Position</b>	<b>Reactivity in Position 10 W [β]</b>	<b>Experimental rod value [β]</b>
<b>Shim Rod</b>	200	0,95	2,5
<b>Regulating Rod</b>	50	0,14	1,2
<b>Transient Rod</b>	499	0	2,1

<b>Core Excess Reactivity at 10 W [β]</b>	2,585
---	-------

Table 5.6: Experimental data from the core excess reactivity measurement on January 1<sup>st</sup> 2013.

### 5.3.2 Simulation of the Core Excess Reactivity

The Serpent reactor model in Core I configuration, previously benchmarked against the calibration of the control rods, can be used to simulate the excess reactivity experiment. The densities and structures of the control rods stay the same throughout all simulations and only their positions change. Instead of being fully inserted or fully

removed from the core, the shim and regulating rod hold positions partially extracted from the core according to the experiment (see figure 5.5). Position 499 represents the rod totally removed from the core, while position 0 refers to the rod being completely inserted and covering the active part of the core.

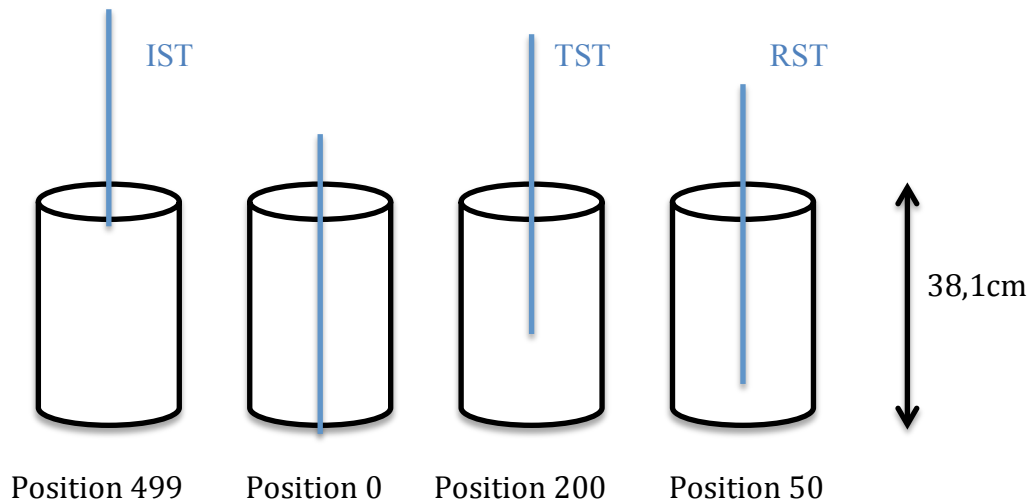


Figure 5.5: Schematic diagram of the control rods, i.e. Transient rod (IST), Shim rod (TST) and Regulating rod (RST), in their positions inside the active core used for the core excess experiment.

The simulation itself is performed for one rod at a time. While the particular control rod is brought into the right position the other two are removed from the core and the simulation is run in  $k$ -eigenvalue criticality source mode.

To calculate the worth of the rod in the respective position, the reactivity found in the simulation has to be subtracted from the reactivity of the configuration with all rods extracted. This leads to the remaining amount of positive reactivity that is still inside the core and could be exceeded by fully removing the control rod. After repeating the simulation and calculation for the other control rods the total core excess reactivity can be summed up according to (5.3).

### 5.3.3 Comparison of Simulation and experimental Data

The simulation and experiment results for the Core I excess reactivity are presented in table 5.7. It is divided into two separate tables. The first one displays the data for the excess reactivity of the control rods and the second one refers to the total core excess reactivity of the given core configuration at 10 W.

The deviation of the control rod excess reactivity simulation lies within 8% to 12% compared to the simulation. The total discrepancy of the Serpent core excess simulation sums up to 15%.

		<b>Shim Rod Pos. 200</b>	<b>Regulating Rod Pos. 50</b>
<b>Serpent Simulation Output</b>	$k_{\text{eff}}$	1,006210	1,011170
	$\rho$ [PCM]	0,006172	0,011047
	$\rho$ [\$]	0,845435	1,513234
<b>Serpent CR Excess</b>	$\Delta\rho_{\text{Serpent}}$ [\$]	1,820818	1,153019
<b>Experimental CR Excess</b>	$\Delta\rho_{\text{exp}}$ [\$]	1,61	1,06
	$\Delta\rho_{\text{exp}}/\Delta\rho_{\text{Serpent}}$	88,42%	91,93%

	<b>Core Excess Reactivity [\$]</b>
<b>Serpent</b>	2,974
<b>Experiment</b>	2,585
<b>Discrepancy</b>	<b>-15,04%</b>

Table 5.7: The upper part of the table displays the excess reactivity of each control rod and its agreement to the experimental value. The lower part describes the total core excess reactivity of the core configuration.

There can be many reasons for the discrepancy between reality and simulation. Material-based error sources can be impurities in the reactor elements, especially the fuel elements and control rods or the impact of a generated or decaying reactor poison.

In addition several simplifications of the real situation have to be made to perform a simulation. The biggest simplification in Serpent was the assumed operational time of the reactor, during which the fuel was burned. The TRIGA Mark II Reactor Vienna is usually operated from Monday to Friday from 9 a.m. to 4 p.m. and shut down during the nights and holidays. Simulating a schedule like that would require one depletion step for each day in operation and one decay step for every time the reactor is shut down. In order to cover a time period of half a year or more a disproportionately big amount of calculation time and processor performance would be required. Therefore operational days were combined to a longer period of time where the reactor was operated at a certain power level without interruption. The same thing was done with the time the reactor was shut down and the fuel decays. So instead of hundreds of steps the calculation was reduced to a few steps that last for a longer period of time. The downside to the optimized simulation efficiency is the decline in accuracy of the gained results.

For this burnup simulation the time period from 2013-01-21 to 2013-07-22 has been divided into two intervals. The first one represents operation at 250 kW for 21,47 days and the second one the decay time of 160,52 days. This simplification contributed to the error as well.

The deviation of the control rods in the given positions also has to be taken into account regarding the calibration curves of the control rods (figure 5.3). While the area below the simulation curve, i.e. the total worth of the rod, fits the measurement very well, the curve itself does not always fit each single measurement point. Further rod calibration simulations suggest, there is a certain offset in the simulation that is compensated for throughout the calibration curve.

As mentioned above, the aim of this thesis is to compare control rod worth and core excess reactivity results throughout four consecutive core configurations. Each core builds on the accuracy of the previous one and any preceding errors run into the ensuing calculations. Instead of a discrepancy of 15%, the best starting point for the next simulations would be a precise first core reproduction. As this is not the case, another option would be to investigate the discrepancy of the first core closely and to introduce the mentioned offset of the regulating and the shim rod. The idea is that this offset remains constant throughout all following simulations. In order to determine the respective accuracy of each calculation, the offset can be added to the gained values for  $k_{eff}$  to correct the initial shift of the results for Core I.

The control rod excess reactivity simulation results including the offsets  $\Delta k$  are presented in table 5.8.

		<b>Shim Rod Pos. 200</b>	<b>Regulating Rod Pos. 50</b>
<b>Serpent Simulation Output</b>	$k_{eff} + \Delta k$	1,007771	1,011865
	$\rho$ [PCM]	0,007711	0,011726
	$\rho$ [\$]	1,056253	1,606253
<b>Serpent CR Excess</b>	$\Delta\rho_{Serpent}$ [\$]	1,610000	1,060000
<b>Experimental CR Excess</b>	$\Delta\rho_{exp}$ [\$]	1,61	1,06
	$\Delta\rho_{exp}/\Delta\rho_{Serpent}$	100,00%	100,00%
<b>Offset</b>	$\Delta k$	0,001561	0,000695

Table 5.8: Excess reactivity of the control rods in perfect agreement with the measurement. The difference between  $k_{eff} + \Delta k$  and the original  $k_{eff}$  in table 5.6 is the offset  $\Delta k$ .

## 5.4 Burnup Calculation

As described in section 2.6, fuel burnup or fuel utilization, is a measure of how much energy is extracted from a nuclear fuel and a measure of fuel depletion. As fuel nuclei are continuously consumed and decaying, reactor operation is always accompanied by significant isotopic changes in the fuel elements. The study of these isotopic changes can be divided into long-term kinetics, describing phenomena occurring over months and years, and short or medium-term kinetics. The former are focusing on arising effects that last for a few hours or days, for example neutron poisoning or spatial oscillations.[3]

The burnup calculation is the central key to analyzing the time evolution of the fuel. It simulates the reactor being in operation at a defined power level over a certain period of time. During the operational intervals Serpent calculates the transmutation rates with which the fissile components of the fuel decay into further elements. It also provides the updated fuel composition of the fuel elements after each burning interval.

The burning intervals are interrupted by decaying intervals that represent the shut down state of the reactor. In the course of these decaying intervals the fuel composition is calculated and updated again by Serpent, due to the possibly exceeded half-life of some isotopes.

### 5.4.1 Burnup Intensity

All three figures 3.3, 5.1 and 5.6 display the same first core setting, but illustrate different properties of the configuration. While figure 3.3 provides information on the location of elements inside the core, figure 5.1 emphasizes on the composition of each core element.

Serpent offers a possibility to visualize the neutronics in thermal systems by plotting the fission power and thermal flux distributions into one file. This so-called mesh plot of the first core configuration is shown in figure 5.6.[4]

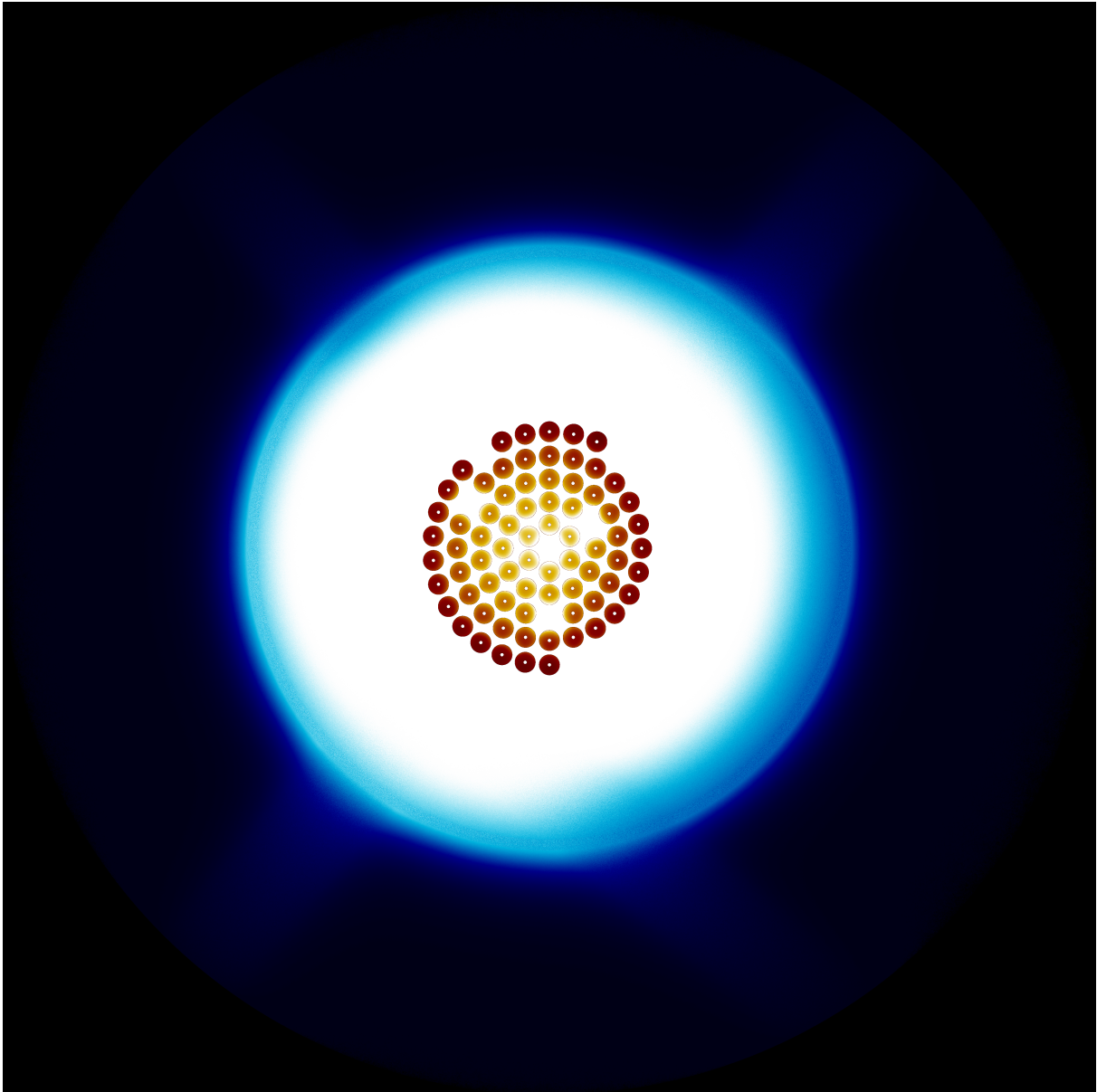


Figure 5.6: Mesh plot of the first core configuration to demonstrate the fission power and thermal flux distributions. The warm color scheme represents the relative fission power. The control rods are pulled out completely for the burnup simulations. The X-shaped blue rays indicate the neutron beam tubes of the facility.

The cold white and blue shades represent the relative thermal neutron flux inside the reactor core, which peaks in the center of the core and the fuel element rings surrounding it. The flux decreases with rising radial distance from the center, is reflected by the graphite and disappears in the concrete shielding.

Due to the varying intensity of the flux within the core, the fuel elements are exposed to a different amount of thermal neutrons according to their position in the core. A higher flux means that the relative fission power of the fuel elements increases and that the fuel depletion or burnup is at its maximum. Those high fission power regions are colored in a bright yellow, whereas the colors of the lower burnup regions transition into a darker

red. In conclusion the expected burnup results for operating the reactor for a certain time period, will be different according to the radial distance to the center. Additionally the fuel elements in Core I presented various amounts of uranium in the beginning, due to the slight burnup they experienced before the fuel element exchange, which has influence on the reactivity as well.

### 5.4.2 Calculation time intervals

Core I was in operation from 2013-01-21 to 2013-07-22, typically Monday to Friday 7 hours a day with possible exceptions. This corresponds to 515,436 operational hours during 162 elapsed days. As explained in chapter 5.3.3, it would be too elaborate and time intense to consider each single operational and shut down hour in the simulation. Instead the time period was divided into three sections and six calculation steps:

- 2013-01-21 to 2013-04-02: The first section covers 71 days and 270,244 operational hours. That means that the first step is a burnup interval at 250 kW for 11,260 days followed by a decay interval for 59,74 days at 0 W power.
- 2013-04-02 to 2013-06-03: The second section lasts for 62 days and covers 141,59 operational hours. The simulation consists of 5,9 days at 250 kW power and an ensuing decay time of 56,1 days.
- 2013-06-03 to 2013-07-22: The last time interval covers 49 days and 103,6 operational hours. The burning process is performed over 4,32 days and the final decay interval lasts for 44,68 days.

Date	Burning Interval [d]	Decay Interval [d]	Total [d]
2013-01-21 to 2013-04-02	11,26	59,74	71
2013-04-02 to 2013-06-03	5,9	56,1	62
2013-06-03 to 2013-07-22	4,32	44,68	49

Table 5.9: The calculation steps of the Serpent Burnup simulation for Core I.

The composition outputs after the final decay step on July 22<sup>nd</sup> are the final results of the simulation of Core I and give information on the changes in the fuel element compositions throughout the operational time of the core. These results indicate the fuel element compositions at the start of the following core.

There is no possibility to directly compare the results of the burnup calculation to the actual measurement of the burnup of each fuel element in the core. Nevertheless the simulation will still be evaluated, as the new core is based on its results and undergoes examination.

## References Chapter 5

- [1] Böck, H., Villa, M.: Praktische Übungen am Reaktor, Vienna University of Technology 2005, AIAU 25315
- [2] Glasstone, S.: Principles of nuclear reactor engineering. Van Nostrand, Princeton, NJ 1955 (IX, 861).
- [3] Lamarsh, J.: Introduction to Nuclear Engineering. Prentice Hall 2001  
ISBN 0-201-82498-1
- [4] Leppänen, J.: Serpent – a Continuous-energy Monte Carlo Reactor Physics Burnup Calculation Code. User's Manual, 2015

# 6.

## Core II and Core III, 2013-07-22 to 2014-04-14

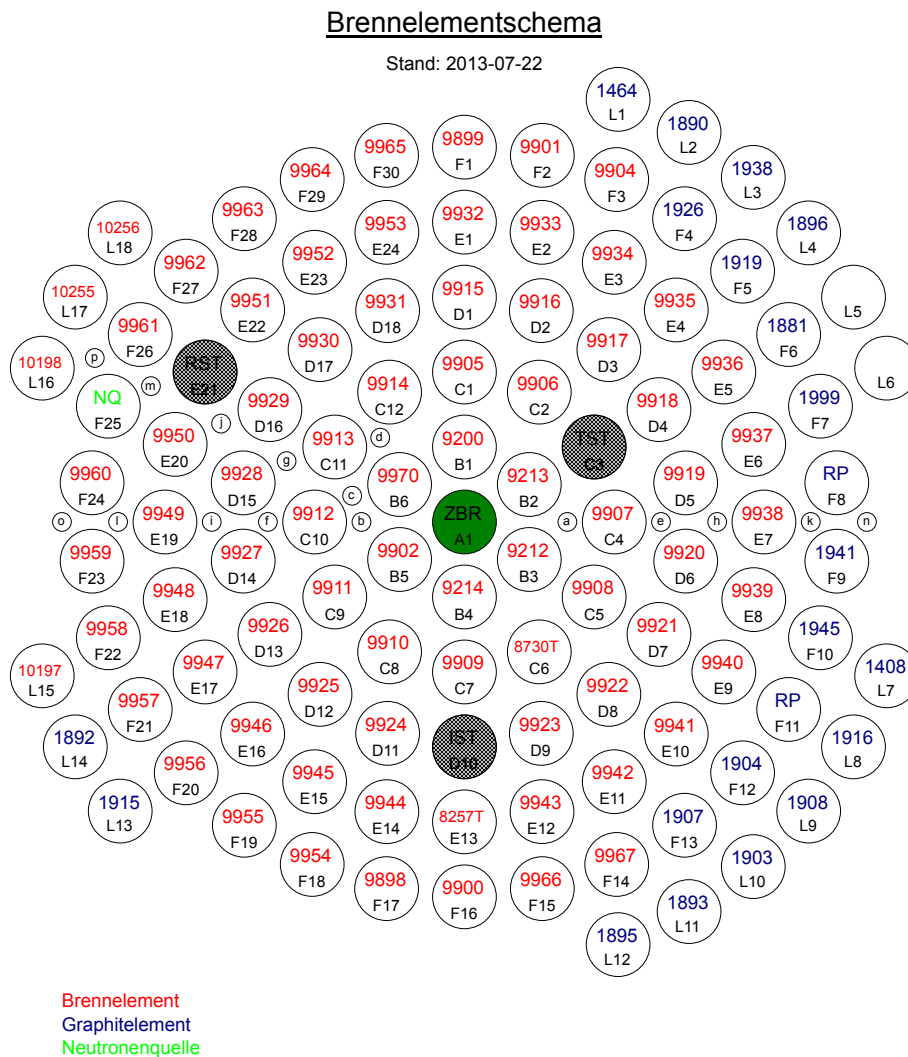


Figure 6.1: Configuration of the Core II

On July 22<sup>nd</sup> 2013 the second core configuration of the TRIGA Mark II reactor Vienna went into operation. It consisted of 74 fuel (FE) and 8 graphite dummy elements (DE).

On October 4<sup>th</sup> 2013 the second core configuration was updated to the third core configuration, where two fuel elements and graphite elements in ring F switched position. That change didn't affect the reactivity of the core, because the fuel elements remained in the same ring. However, there is some experimental benchmark data from January 2014 to validate the accuracy of the core. Up to that date the second core was in operation for a slightly longer period of time than the third core. Due to the similarity of the two configurations, they were combined for the *burnup calculation* to just one that corresponds to the second core in figure 6.1. After merging the cores for the simulation, the setting was in operation until 2014-04-14.

The configuration of Core III (see figure 6.2) was recreated in Serpent as well. It is used to obtain results for the *rods worth and the core excess reactivity simulation*, because that core was in operation during the experiment in January 2014.

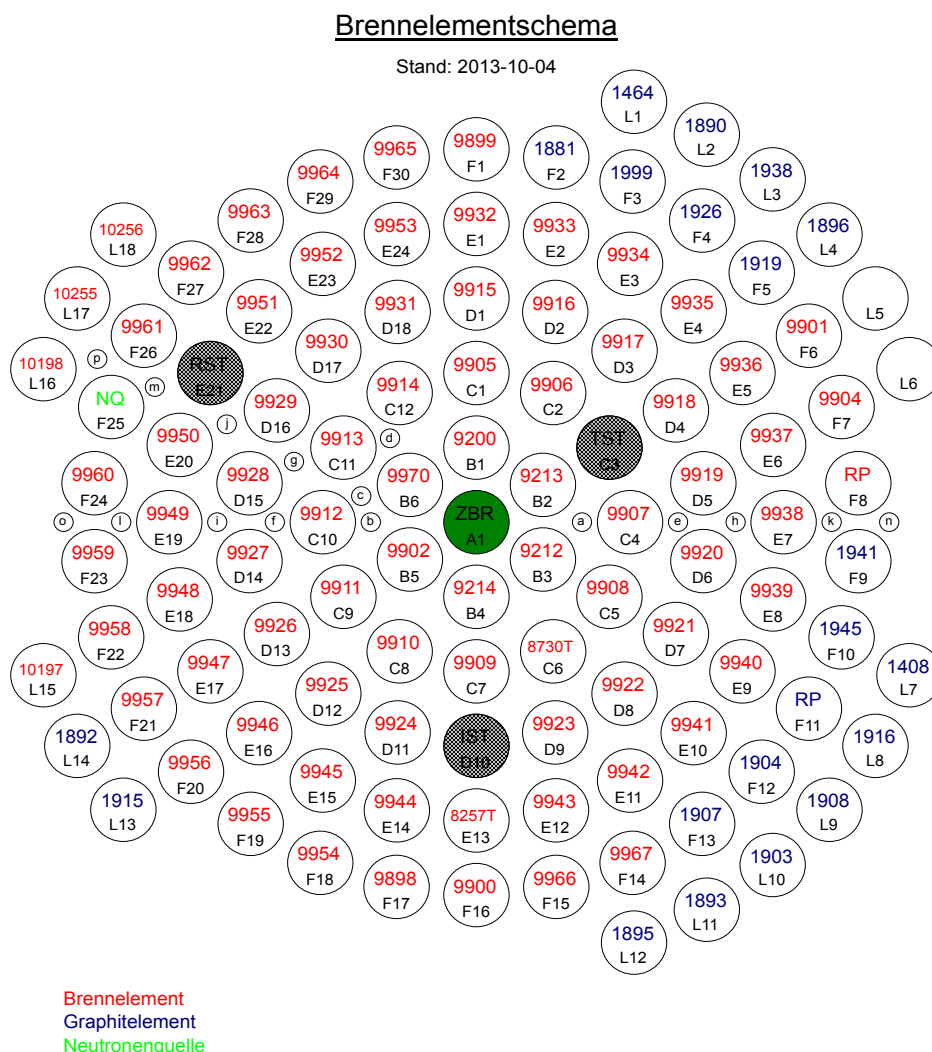


Figure 6.2: Configuration of Core III.

## 6.1 Update of the fuel element configuration

The input file of Core II configuration was based on the structure of Core I, because most fuel elements stayed in the exact same position. In addition two more fuel elements with an original burnup of 0,53% were added in positions F15 and F16. Besides, in the scope of moving the neutron source form F28 to F25, three fuel elements in the F ring were moved to the adjacent position. Table 6.1 presents the differences between Core I, Core II and Core III.

21.01.2013	Core I		Fuel Element	Position	
22.07.2013	Core II	<b>added FE</b>	9966	F15	
			9967	F14	
		<b>moved FE</b>	9963	from F27	to F28
			9962	from F26	to F27
			9961	from F25	to F26
		<b>moved NQ</b>	Neutron Source	from F28	to F25
04.10.2013	Core III	<b>moved FE</b>	9901	from F2	to F6
			9904	from F3	to F7
		<b>moved DE</b>	1881	from F6	to F2
			1999	from F7	to F3

Table 6.1: Differences in the configurations of three ensuing cores.

### 6.1.1 Changes in the fuel composition

Besides the arrangement of the fuel elements, especially their compositions have changed compared to the Core I. After the fuel was burned in Core I over a time period of a total 182 days, there is a slight depletion of uranium-235 and arising from its decay numerous other nuclides became part of the fuel composition. To get the exact composition of all elements in Core II, each fuel element has to be updated with the respective results in the material lists of the burnup calculation of core I.

The mentioned burnup material lists contain approximately 260 isotopes appearing in different quantities and with varying half-lives. Only the elements with the biggest impact on the reactivity are adopted into the new fuel composition. That includes the updated amounts of the original components (see table 6.3) and all isotopes of the fissile elements uranium (Z=92) and plutonium (Z=94), which occur in reasonable amounts with atomic densities  $> 10^{-10} \frac{10^{24}}{cm^3}$ .

### 6.1.2. Neutron poisons in the composition

Among the isotopes produced while operating the reactor, there are some neutron poisons as well. As described in section 2.4.4, poisons are characterized by very high thermal neutron absorption cross-sections  $\sigma_a$  and have crucial influence on the reactivity and the state of the reactor. Therefore they have to be added to the fuel element composition too.

The consideration, which poisons to include, emphasizes on three parameters. The first one is the selection of the isotopes with the highest absorption cross-sections for thermal neutrons. The second one examines the atomic density of each poison isotope in the composition, rejecting those with atomic densities  $< 10^{-15} \frac{10^{24}}{cm^3}$ .

The final step is to check the eligible poisons for their half-lives. It should be considered, if a reduction of reactivity has to be expected for the next start up and the typical time their presence could affect reactor operation. Figure 6.3 demonstrates the time evolution of four exemplarily chosen reactor poisons with different  $\sigma_a$  and half-lives listed in table 6.2.

Isotope	Absorption Cross Section [ $10^{-24} \text{ cm}^2$ ]	Half-Life
Xe-135	$2650000 \pm 110000$	9,14 h
Sm-149	$40140 \pm 600$	$2 \cdot 10^{15}$ a
Pm-148	$2000 \pm 1000$	5,370 d
Cs-134	$140 \pm 12$	2,0648 a

Table 6.2: Properties of four reactor poisons depicted in Figure 6.2.

In case of the TRIGA Mark II in Vienna and for the purpose of this work, i.e. evaluation of long term effects to reactor operation, half-lives shorter than a few days don't need to be taken into consideration for the fuel composition in the Serpent simulation.

The poisons actually chosen for being implemented into the fuel element composition and their atomic densities are given alongside the other isotopes at 300K in table 6.3.

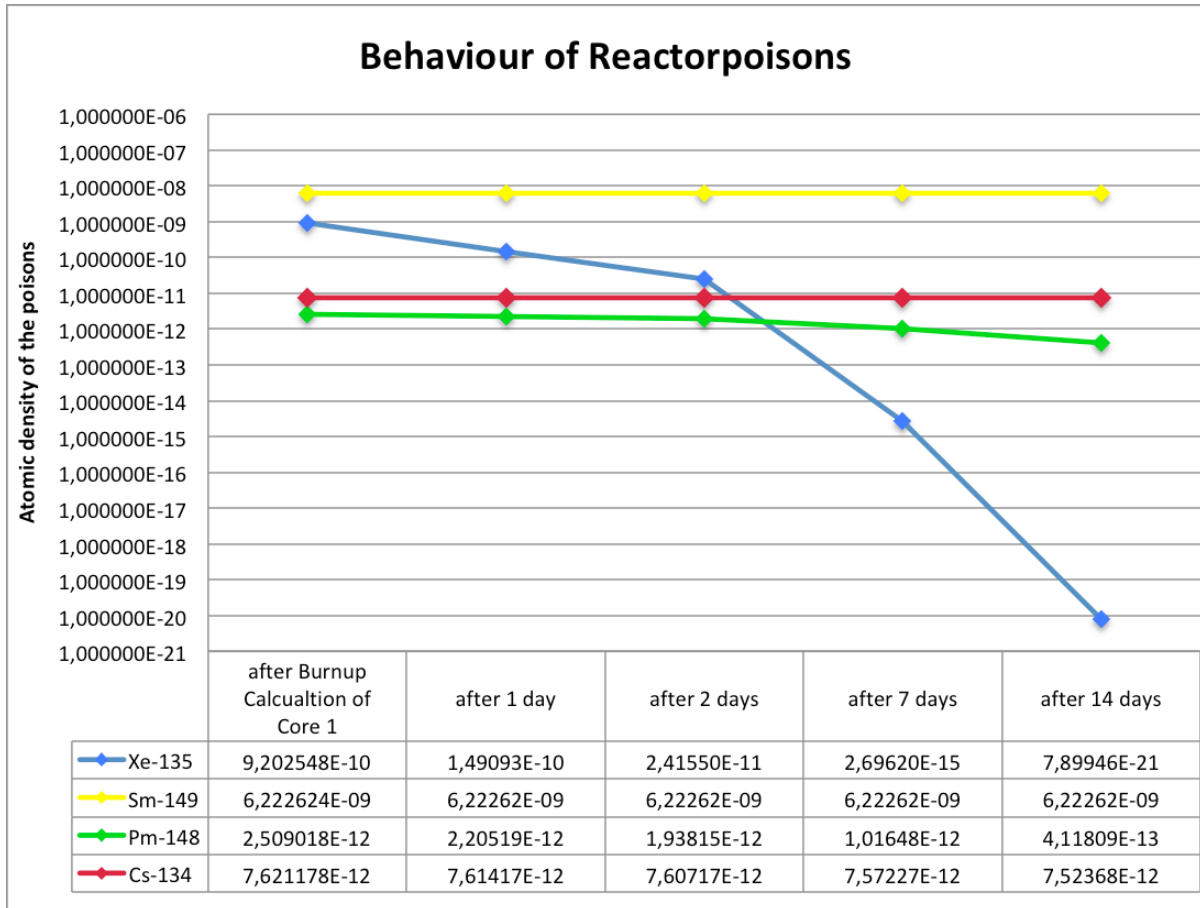


Figure 6.3: Medium-term time evolution of four different reactor poisons.

Starting fuel composition Core I	Fuel Composition Core II
Atomic density from composition 9,31674126480975E+12	Atomic density from composition 9,31681677276183E+12
Atomic density of Isotope at 300 K	Atomic density of Isotope at 300 K
H <sup>1</sup> 1001.03c 5.55939928056885E-02	H <sup>1</sup> 1001.03c 5.55938928807850E-02
Zr <sup>90</sup> 40090.03c 3.63022693761424E-02	Zr <sup>90</sup> 40090.03c 3.63022497071645E-02
U <sup>235</sup> 92235.03c 2.55265837558185E-04	U <sup>235</sup> 92235.03c 2.54357536885008E-04
U <sup>238</sup> 92238.03c 1.01588462870853E-03	U <sup>236</sup> 92236.03c 1.43601884729760E-07
	U <sup>238</sup> 92238.03c 1.01580826590545E-03
	Pu <sup>239</sup> 94239.03c 7.36114469347901E-08
	Cd <sup>113</sup> 48113.03c 1.04893543010917E-10
	Sm <sup>149</sup> 62149.03c 6.92433786269216E-09
	Sm <sup>151</sup> 62151.03c 3.12949303250506E-09
	Eu <sup>151</sup> 63151.03c 8.55433035810799E-12
	Gd <sup>155</sup> 64155.03c 1.20086907969634E-11
	Gd <sup>157</sup> 64157.03c 3.25683494354736E-11

Table 6.3: Left side: Original composition of FE 9214 in the first core at 300K. The first two numbers indicate the atomic number Z and the following three numbers the isotope of the element. Right side: New composition of FE 9214 in the second core at 300K. The red colored lines mark the fissile isotopes and the blue colored lines indicate the chosen neutron poisons and their atomic densities.

## 6.2 Burnup Calculation

The pre-burnup-calculation-considerations for Core II are basically the same as for Core I. Due to the changes in the core configuration, two of the representative fuel elements for which the burnup gets calculated, have to be slightly changed in the F-ring and instead of 72 they are now representing 74 fuel elements.

Core II was in operation for 266 days from 2013-07-22 until 2014-04-14. That corresponds to 783,5 operational hours or rather 32,6 operational days. Some experimental measurements were taken after 509,2 operational hours on January 7<sup>th</sup> 2014. In order to simulate those experiments, it is necessary to know the exact fuel composition on that date.

For the Serpent burnup calculation the time period was divided into two sections and four calculation steps:

- 2013-07-22 to 2014-07-01: The first section covers a period of 169 days. It consist of a burning interval at 250 kW power that lasts for 21,2 days, followed by a decay interval for 147,8 days at 0 W. The material burnup results after this decay step are used for the fuel element composition of the rod worth and core excess simulation.
- 2014-07-01 to 2014-04-14: The other section lasts for 97 days from the Measurement until the changing of the core configuration in April 2014. The burning interval covers a period of 11,2 days at 250 kW. The ensuing decay step lasts for 85,6 days. The output data for the last decay interval provide the composition results after Core II. This will be the starting composition of the next core.

Date	Burning Interval [d]	Decay Interval [d]	Total [d]
2013-07-22 to 2014-07-01	21,2	147,8	169
2014-07-01 to 2014-04-14	11,2	85,6	97

Table 6.4: The calculation steps of the Serpent Burnup simulation for Core II.

### 6.3 Worth of the Control Rods

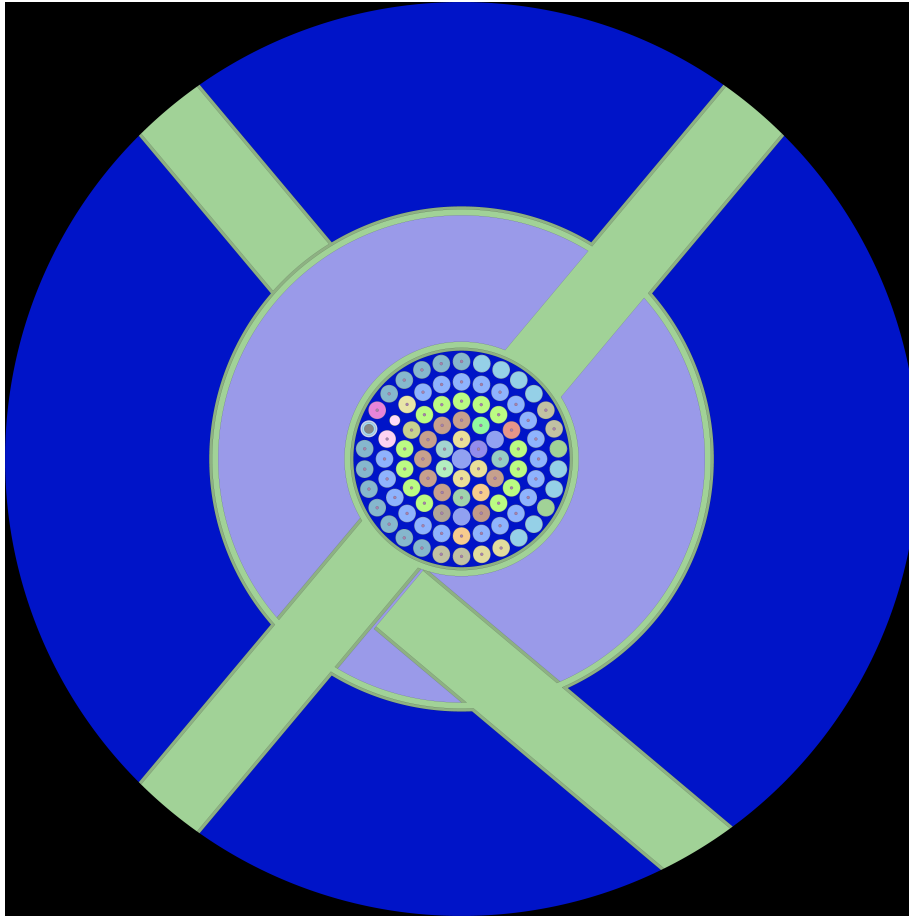


Figure 6.3: Core III configuration during the rod worth simulation of the regulating rod. Elements of the same colour consist of the same fuel composition or material. The X-shaped green outlets are the beam tubes of the facility.

The experimental determination of the control rod worth and the calibration curve took place in January 2014. At that time core configuration III was already in operation and used for the measurement. The experimental procedure was performed at 10 W as usual (see section 5.2).

In order to achieve simulation results as coherent as possible with the measurements, it is necessary to align the framework conditions of the simulation to those of the experiment. Therefore Core III had to be recreated in Serpent, using the updated composition from the burnup calculation of Core II on January 7<sup>th</sup> for the fuel elements.

Figure 6.3 displays the configuration of Core III during the rod worth Simulation of the regulating rod. In the plot the shim and transient rod are entirely extracted from the core and the regulating rod is fully inserted.

### 6.3.1 Comparison of Simulation and experimental Data

Table 6.5 presents the control rod worth simulation data of Core II and the according agreement with the experimental measurements in the blue colored *Experimental Rod value*-line.

		All Rods extracted	Transient inserted	Regulating inserted	Shim inserted
<b>Serpent Simulation Output</b>	$k_{\text{eff}}$	1,015560	1,000370	1,007700	0,996613
	$\rho$ [PCM]	0,015322	0,000370	0,007641	
	$\rho$ [\$]	2,098849	0,050666	1,046735	
<b>Serpent Rod value</b>	$\Delta\rho_{\text{Serpent}}$ [PCM]		0,014952	0,007680	
	$\Delta\rho_{\text{Serpent}}$ [\$]		2,048183	1,052114	
<b>Experimental Rod value</b>	$\Delta\rho_{\text{exp}}$ [\$]		2,44	1,14	2,60
	$\Delta\rho_{\text{exp}}/\Delta\rho_{\text{Serpent}}$		119,13%	108,35%	

Table 6.5: Experimental and simulation results for the control rod worth of Core II.

Regarding the Core II, the reactivity of the configuration with all control rods pulled out of the core decreased compared to Core I. This is a consequence of the changed core configuration with the added fuel elements and the updated fuel composition, holding a smaller share of fissile U-235.

Comparing the control rods worth, the simulation of the regulating rod fits the experimental results within 8%.

The transient rod presents a deviation of 19%, which is 6% more compared to its deviation in Core I.

It's not possible to make any reliable statement about the shim rod, as the configuration did not get critical. That implies that the shim rod has a stronger absorbing effect in the simulation than it actually has in reality. Considering the differences to Core I, this can be partially explained by the new fuel element setting in ring F: In Core III the fuel elements 9901 in F2 and 9904 in F3 exchange position with the dummy elements in F6 and F7. As the new positions are now much closer to the shim rod, the control rod is exposed to a bigger neutron flux arising from the fission in the fuel elements. Therefore

the shim rod absorbs a bigger amount of neutrons and prevents criticality of the configuration.

The situation is similar for the newly added fuel elements 9966 and 9967 in positions F15 and F14. The additional fissile material close to the transient rod probably also has a neutron absorption-increasing impact on the control rod. However the impact is not directly noticeable looking at the criticality of the transient rod simulation of Core III.

### 6.4 Core III Excess Reactivity

The core excess reactivity measurement was performed during the operation of Core III in January 2014. The experimental procedure is exactly the same as for Core I in section 5.3.1.

The transient rod gets pulled out of the core completely and the shim and regulating rod are extracted partially, until the reactor reaches criticality at 10 W. The positions of the control rods, the according reactivity and the total rod worth are displayed in table 6.6. The total core excess reactivity is the sum of the excess reactivity values of the single control rods.

	Rod Position	Reactivity in Position 10 W [β]	Experimental Rod value [β]
Shim Rod	190	0,97	2,60
Regulating Rod	170	0,41	1,14
Transient Rod	499	0	2,44

<b>Core Excess Reactivity at 10 W [β]</b>	<b>2,36</b>
---	-------------

Table 6.6: Experimental Data from the core excess measurement.

Regarding the simulation the main steps are the same as for Core I. The excess reactivity is calculated for each control rod at a time running serpent in  $k$ -eigenvalue criticality source mode. The result  $\Delta\rho$  has to be subtracted from the reactivity of the configuration with all rods pulled out and then the gained values need to be added up to the core excess reactivity.

### 6.4.1 Comparison of Simulation and experimental Data

Table 6.7 is divided into two parts and presents the results of the excess reactivity of the control rods plus its agreement and the total core excess reactivity of the core and its deviation from the measurement.

The steady offset determined in Core I already went into consideration within the shown results. While the simulation itself provided  $k_{eff}$ , the offsets of the regulating and the shim rod were added to the gained values and the modified  $k_{eff} + \Delta k$  was further processed.

		<b>Shim Rod Pos. 190</b>	<b>Regulating Rod Pos. 172</b>
<b>Serpent Simulation Output</b>	$k_{eff}$	1,0017	1,00951
	$k_{eff} + \Delta k$	1,003261	1,010205
	$\rho$ [PCM]	0,003250	0,010102
	$\rho$ [\$]	0,445201	1,383792
<b>Serpent CR Excess</b>	$\Delta\rho_{Serpent}$ [\$]	1,653648	0,715057
<b>Experimental CR Excess</b>	$\Delta\rho_{exp}$ [\$]	1,63	0,73
	$\Delta\rho_{exp}/\Delta\rho_{Serpent}$	98,57%	102,09%

	<b>Core Excess Reactivity [\$]</b>
<b>Serpent</b>	2,368704
<b>Experiment</b>	2,360000
<b>Discrepancy</b>	<b>-0,37%</b>

Table 6.7: The first table displays the excess reactivity of each control rod and its agreement with the experimental value. The second table describes the total core excess reactivity of the core configuration.

The gained results for the excess reactivity of the control rods including the offsets lie within a very good agreement of 2%. The configuration with the shim rod in position 190 was critical straightaway and the influence of the additional fuel elements only resulted in a slightly higher excess reactivity of the shim rod.

The good results for the excess reactivity values of the control rods lead to an even better agreement of the measurement and the simulation of the total core excess reactivity. The calculated value of 2,369 \$ fits the experimentally determined value of 2,360 \$ almost perfectly.

The experimental tests of the core configuration, i.e. calibration of the control rods and excess reactivity measurement, are usually performed once a year. These measurements provide the data that are used to evaluate the simulations and to compare the calculations to. During time intervals in-between the experiments, there is no available information about the evolution of the core and single burning steps or calculated fuel compositions cannot be verified right away. Therefore it is even more important to obtain good agreement in the simulation results for the measurements in January, because a good accuracy implies the properness of the previously performed calculation steps.



Core IV is the last core configuration calculated within the scope of this thesis. It went into operation on April 14<sup>th</sup> 2014 and served for 892,4 operational hours until April 2015. The core was critical at 250 kW with 74 fuel elements (*FE*) and 8 dummy elements (*DE*).

There is some experimental data of the rod worth measurement available from January and April 2015 and the core excess measurement was performed on March 30<sup>th</sup> 2015. Even though Core IV actually stayed in the reactor until February 2016, April 2015 was the last time it went into operation. After that, the reactor remained shut down for nearly a year, due to the refurbishment works on the Instrumentation and Control System of the reactor.

## 7.1 Update of the fuel element configuration

The setting of the Core IV is basically equal to Core III and the fuel elements 9901 and 9904 are still in positions F6 and F7. The only thing that has changed, is that FE 9959 had been removed from the core and FE 9968 with 0,53% burnup has been inserted into F23 position. Table 7.1 is an extension of Table 6.1 and presents the differences of Core III and Core IV.

		Fuel Element	Position		
14.04.2014	4th configuration	<b>removed FE</b>	9959	from F23	to tank
		<b>added FE</b>	9968	F23	

Table 7.1: Changes from Core III to Core IV.

### 7.1.1 Changes in the fuel composition

Updating the fuel element composition of the Core IV was done analogously to updating the composition of Core II in section 6.1.2. The final burnup calculations after 783,5 operational hours of Core II provide the new material compositions of the representative fuel elements chosen for the burnup simulation. These final material lists are the starting composition for all fuel elements in Core IV.

Just like before produced reactor poisons and fissile isotopes have to be especially taken into account. The lists of isotopes to be considered in the simplified updated fuel composition were chosen under the same considerations and are the same as for

Core II. The new starting composition is displayed as an example for FE 9214 in table 7.2.

The only exception in Core IV is the lately added FE 9968. It starts off with the composition of a fresh fuel element, but with the accordingly reduced fraction of U-235 and is listed in table 5.1.

Fuel Composition Core IV	
Atomic density from composition 9,31692953446697E+12	
Atomic density of Isotope at 300 K	
H <sup>1</sup>	1001.03c 5.559471600392E-02
Zr <sup>90</sup>	40090.03c 3.63028564317058E-02
U <sup>235</sup>	92235.03c 2.53006447183620E-04
U <sup>236</sup>	92236.03c 3.57778756353785E-07
U <sup>238</sup>	92238.03c 1.01571207412675E-03
Pu <sup>239</sup>	94239.03c 1.82385602623653E-07
Cd <sup>113</sup>	48113.03c 2.26618316715596E-10
Sm <sup>149</sup>	62149.03c 1.28600398602003E-08
Sm <sup>151</sup>	62151.03c 7.44784464532400E-09
Eu <sup>151</sup>	63151.03c 4.31088705337453E-11
Gd <sup>155</sup>	64155.03c 3.46191636552643E-11
Gd <sup>157</sup>	64157.03c 4.85544888804677E-11

Table 7.2: New composition of FE 9214 in the Core IV at 300K. The red colored lines mark the fissile isotopes and the blue colored lines indicate the chosen neutron poisons and their atomic densities.

## 7.2 Burnup Calculation

In Core IV 21 fuel elements are chosen for the burnup calculation. That is one more than for Core II, because one new fuel element was added. All other considerations before the burnup simulation were the same as for the previous cores (see chapter 5.4).

Until the rod worth and excess reactivity measurements on March 30<sup>th</sup> 2015 core four had been in operation at 250 kW for 892,4 operational hours or 37,2 operational days. During April 14<sup>th</sup> 2014 and the date of the measurement 350 days elapsed. As the reactor was shut down in April 2015 the simulation of the fuel elements burnup stops at that time. The long decay step of 333 days until the reactor went into operation again in February 2016 has not been taken into account and the time period covered in this thesis ends on April 2<sup>nd</sup> 2015.

As the day of the measurements is equal to the last day of operational time covered by the burnup calculation, this simulation did not need to be divided and consists of only one section:

- 2014-04-14 to 2015-04-02: The entire burnup calculation covers a period of 353 days and starts with a burning interval lasting for 37,2 days at a power level of 250 kW. The remaining 315,8 days are covered by the decay interval at 0 W power. The composition of the fuel elements after this last decay step can be considered the final result of this thesis. They could be the starting fuel composition of future core simulations regarding the reactor after the I&C-System exchange in 2016.

### 7.3 Worth of the Control Rods

The measurement of the worth of the control rods took place on two different dates at the beginning of January and at the beginning of April 2015. The experimental procedure is the same as for the two previous cores and was performed for each rod at a time at a power level of 10 W.

Simulating the state of the Core IV at the beginning of April 2015 requires updating the fuel composition. The update is based on the gained material composition lists from the last decay step of the burnup calculation.

#### 7.3.1 Comparison of Simulation and experimental Data

		All Rods extracted	Transient inserted	Regulating inserted	Shim inserted
<b>Serpent Simulation Output</b>	$k_{eff}$	1,012380	0,996781	1,004090	0,993062
	$\rho$ [PCM]	0,012229		0,004073	
	$\rho$ [\$]	1,675152		0,557992	
<b>Serpent Rod value</b>	$\Delta\rho_{Serpent}$ [PCM]			0,008155	
	$\Delta\rho_{Serpent}$ [\$]			1,117160	
<b>Experimental Rod value</b>	$\Delta\rho_{exp}$ [\$]		2,03	1,15	2,32
	$\Delta\rho_{exp}/\Delta\rho_{Serpent}$			102,94%	

Table 7.3: Experimental and simulation results for the control rod worth of Core IV on April 1<sup>st</sup> 2015.

The agreement of the calculated worth of the control rods and the measured results are presented in table 7.3. The measurement data is given in the *Experimental Rod value-line*.

The burnup of the fuel causes the reactivity of the core setting with all control rods extracted to decrease. Despite the strong similarity of the configurations of Core IV and Core III and adding a new fuel element, the reactivity of the configuration with all control rods extracted is less than 2\$ for the first time.

The agreement of the simulated and the measured worth of the regulating rod stays within 3%. In comparison with the 8% deviation in Core III the accuracy of the simulation of Core IV has increased significantly considering the regulating rod.

The biggest problem with the simulation is that the configuration neither gets critical for the shim, nor for the transient rod. Therefore no reliable conclusion about the accuracy of these results can be drawn. The reason why  $k_{eff} < 1$ , is probably the same one as described for Core III. Due to the moving or adding of burnable fuel elements near a control rod, the control rod is facing a higher neutron flux and has a stronger absorbing effect. When the neutron absorption gets too strong, the configuration with one rod completely inserted is being prevented from becoming critical.

#### **7.4 Core IV Excess Reactivity**

The core excess reactivity measurement has been performed on March 30<sup>th</sup> 2015 at a power level of 10 W. The procedure of the experiment is analog to the core excess reactivity measurement described for Core I and Core III.

As before, the transient rod is fully removed from the core and the shim and regulating rod are partially inserted to reach criticality. The according reactivity values from the control rod calibration curves can be assigned to the respective rod positions and are displayed in table 7.3, along with the calculated core excess reactivity.

In accordance with Core I and Core III the control rod excess reactivity  $\Delta\rho$  is simulated in Serpent for each rod at a time. After subtracting the gained values from the reactivity when all rods are extracted, the results can be added up to the core excess reactivity.

	Rod Position	Reactivity in Position 10 W [\\$]	Experimental Rod value [\\$]
Shim Rod	220	0,80	2,32
Regulating Rod	182	0,45	1,15
Transient Rod	499	0	2,03

<b>Core Excess Reactivity at 10 W [\\$]</b>	<b>2,22</b>
---	-------------

Table 7.3: Experimental Data from the Core IV excess reactivity measurement on March 30<sup>th</sup> 2015.

### 7.4.1 Comparison of Simulation and experimental Data

Table 7.4 presents the simulation and experimental results of both the control rod excess reactivity and the core excess reactivity.

Regarding the first line of the table  $k_{eff}$  refers to the values originally gained in the simulations. To take the initial deviation of the simulation from Core I into account, the determined offsets (see chapter 5.3.3) are added to the shim and the regulating rod. From that point the modified  $k_{eff} + \Delta k$  is converted and used for the final core excess reactivity calculation.

		Shim Rod Pos. 220	Regulating Rod Pos. 182
<b>Serpent Simulation Output</b>	$k_{eff}$	0,999612	1,006090
	$k_{eff} + \Delta k$	1,001173	1,006785
	$\rho$ [PCM]	0,001171	0,006739
	$\rho$ [\\$]	0,160437	0,923157
<b>Serpent CR Excess</b>	$\Delta\rho_{Serpent}$ [\\$]	1,514715	0,751995
<b>Experimental CR Excess</b>	$\Delta\rho_{exp}$ [\\$]	1,52	0,70
	$\Delta\rho_{exp}/\Delta\rho_{Serpent}$	100,35%	93,09%

	Core Excess Reactivity [\\$]
<b>Serpent</b>	2,266710
<b>Experiment</b>	2,220000
<b>Discrepancy</b>	<b>-2,10%</b>

Table 7.4: The upper table presents the core excess reactivity of the control rods. The second table describes the total core excess reactivity of the fourth core configuration.

Having a closer look at the first table presenting the excess reactivity of the control rods shows a really good agreement of the simulation of the shim rod and the actual measurement results. The value of the shim rod Serpent simulation matches the experimental value within  $< 1\%$ .

As expected regarding all previous simulations of the regulating rod, the excess reactivity simulation reached criticality right away. The agreement is still fair, as deviation stays within 7%.

The final results for the total core excess reactivity calculated from the values of the simulations fit the measurement data with very good agreement, which is a good feedback for all burnup simulations previously performed with the different cores. In fact this demonstrates, that the fuel compositions calculated throughout every earlier configuration properly contributed to the final results. A discrepancy of about 2,10% for the overall core excess reactivity validates the repeated Serpent simulations of many cores to calculate important reactor parameters.

Such good results were achieved with the utilization of a certain offset of  $k_{eff}$ , empirically determined in the reactivity Serpent simulation of Core I. That offset allowed the simulations to start from a point of perfect agreement and was included in all core excess reactivity calculations.

Comparing the discrepancy of the core excess reactivity simulation of Core III (0,37%) and the deviation of Core IV, suggests that a deterioration of about one to two percent was produced during the simulations. That is a remarkably small deviation, considering how many big simplifications were assumed throughout all simulation in between those two results.

After the long break starting in April 2015 the reactor went back into operation with Core V on February 29<sup>th</sup> 2016.

## 8.

### **Burnup and Evolution of U-235**

The final chapter of this thesis emphasizes on the time evolution of the fissile component U-235 of the fuel element composition.

When it comes to discussing the main influences impacting the U-235 depletion of the fuel, one of the two most crucial parameters is the time period for which the reactor is in operation. The longer the burning interval of a core configuration, the more fissile fuel is depleted. The second criterion determining the intensity of the fuel burnup is the actual position of the respective fuel element in the core. The high thermal neutron fluxes in short radial distance to the core center, cause an increase in the relative fission power of the fuel elements and therefore more U-235 is consumed.

When the reactor first went back into regular operation in January 2013 after the fuel element exchange, the fuel element compositions either conformed to fresh fuel or exhibited a slight burnup of up to 1% (see chapter 5.1). The first core was in operation from Monday to Friday seven hours a day for 162 days, the combined second and third core for 266 days and the fourth core for 353 days. That adds up to 781 days the fuel elements had been in operation.

Figure 7.2 and the added table illustrate the time evolution of the atomic density of U-235 in five exemplarily chosen fuel elements. The time evolution covers four different states of the fuel composition at different times:

- The start of Core I in January 2013
- After the operation of Core I in July 2013
- After the operation of Core II/III in April 2014
- After the final operation of Core IV in April 2015, before the reactor was shut down for maintenance.

The discussion of the U-235 burnup during reactor operation is shown for five different fuel elements. They are all located in the same position, but in different rings, continually increasing the radial distance from the center of the core. As the control rods were fully extracted from the core during the burnup simulations, their proximity to the fuel elements does not influence the results. The chosen elements are:

- FE 9200 in position B1; fresh fuel
- FE 9905 in position C1; initially 0,85% burnup
- FE 9915 in position D1; initially 0,74% burnup
- FE 9932 in position E1; initially 0,62% burnup
- FE 9899 in position F1; initially 0,53% burnup

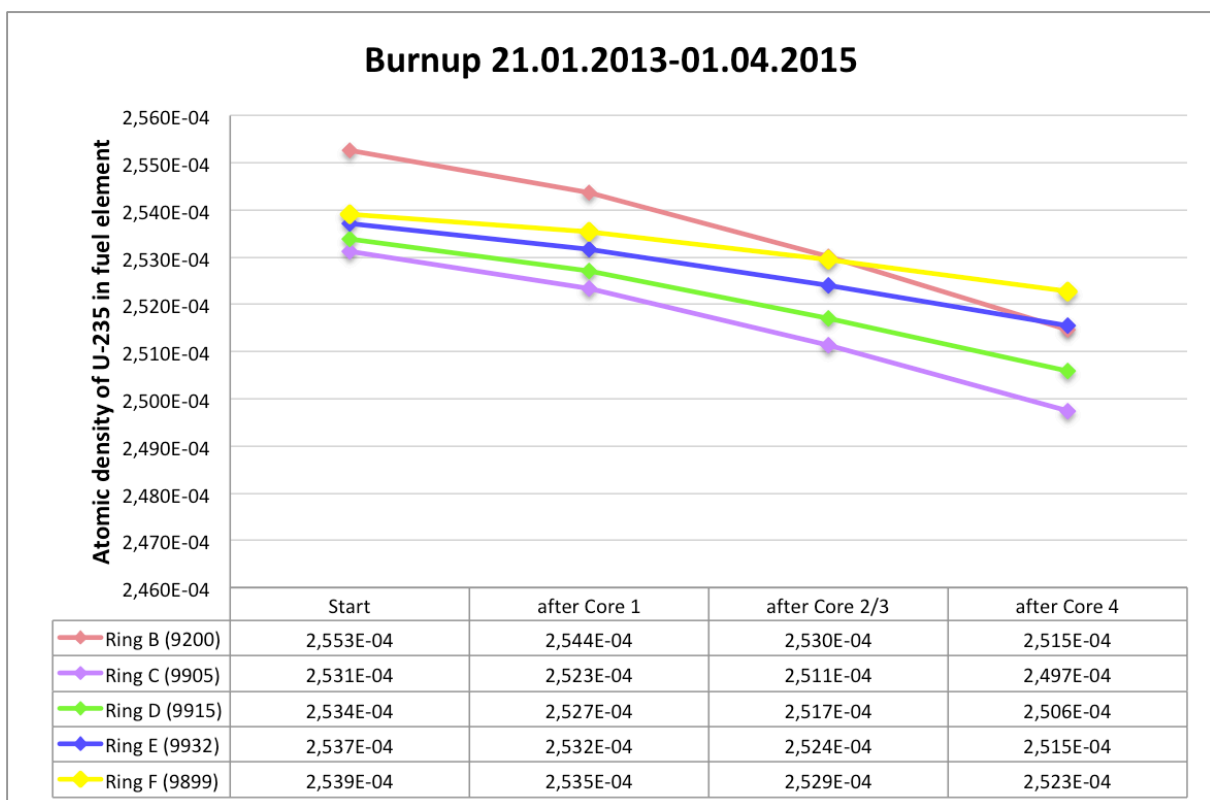


Figure 7.2: Atomic density of U-235 in five fuel elements from different rings in the core after each burnup calculation.

A closer look at the plotted data suggests, that the fuel element in ring B experiences the strongest decrease of uranium-235. The closer the ring of the fuel element is to the center, the higher is its relative depletion in every burning interval.

The amount of fuel consumed during the operation of every core is in direct correlation to the time the reactor was running. Core I was operated for the shortest time and accordingly the decrease of U-235 in each fuel element was less than during the operation of Core II. With 353 days Core IV was by far the longest operated core and therefore shows the biggest reduction of atomic density of U-235.

The final results displaying the overall burnup of the fuel elements from the starting composition to after Core IV in April 2015 are presented in table 7.5.

<b>Fuel Element</b>	<b>Burnup in %</b>
9200	1,4891
9905	1,3371
9915	1,1064
9932	0,8521
9899	0,6426

Table 7.5: Uranium-235 burnup of five representative fuel elements.

In conclusion fuel element 9200 experiences the highest depletion, as it is the closest to the center. Fuel element 9899 is the furthest from the center of the core and has the littlest amount of burnup. The remaining three fuel elements behave accordingly to the radial distance of their location to the center.

## Conclusion

The present thesis describes the evaluation of transmutation rates in the TRIGA Mark II reactor Vienna by the means of the Serpent Burnup Calculation Code and the estimation of the time-evolution of the fuel element composition in a new reactor core configuration. This was done by benchmarking any Serpent simulation results with reactivity measurements that were taken from historical background and performed in the actual reactor core configuration.

The time period that was considered in this work runs from January 21<sup>st</sup> 2013 to April 2<sup>nd</sup> 2015. During this period four core configurations were in operation, called Core I, Core II, Core III and Core IV. In each case the evaluation procedure started with recreating the respective core configuration in the Serpent reactor model and from that point proceeded analogously for every core: Simulations to determine the worth of each control rod were performed and subsequently the obtained values were compared to the results of the experiment. The experiments were carried out in the actual reactor core and good agreement of the results verifies the adjusted model.

The most important comparative value in this thesis was the excess reactivity of each core configuration. Therefore the simulations were performed for each control rod at a time and reproduced the conditions, parameters and control rod positions that were exactly used in the core excess reactivity experiment. The values of the control rods allow calculating the over all core excess reactivity, which again could be compared to the values obtained in the experiment. The discrepancy between the calculated and the experimental excess reactivity determined the accuracy of the Serpent reactor model and the Serpent calculations. All excess reactivity simulation results are presented in table 9.1.

The key consideration in this thesis was the burnup calculation for the operating time of each reactor core configuration. To make this calculation more efficient some simplifications were introduced, e.g. collapsing the operating and decaying time to longer intervals (see chapter 5.3.3). Serpent provided the updated compositions for all fuel elements after each burnup step. The final fuel composition at the end of the operation time of the core constituted the starting composition of the following core.

The results obtained with the Serpent model for the initial configuration Core I (see chapter 5) showed a total discrepancy of the core excess reactivity simulation (2,974 \$)

compared to the experiment (2,585 \$) of 15,04%. The core excess reactivity was calculated by adding the excess reactivity of the partially inserted control rods. The simulation excess reactivity of the shim and regulating rod was in fair agreement with the experiment and the deviation of both lies within 12%. A precise first core reproduction was necessary to investigate the accuracy of the ensuing simulations and therefore an offset was introduced to the regulating and the shim rod. The idea was, that this offset remains constant throughout all following simulations and that it was added to the obtained values for  $k_{eff}$  to correct the initial shift of the results for Core I.

The most crucial considerations for the combined Core II + III (see chapter 6) were updating the fuel element compositions and considering any produced reactor poisons or fissile fuel components. The simulation results for the excess reactivity of the shim rod and the regulating rod were in very good agreement with the experiments with deviations of 1,43% and 2,09%. The total discrepancy of the Core II+III excess reactivity simulation (2,369 \$) compared to the experimental value (2,360 \$) is only 0,37%.

Regarding the final configuration Core IV (see chapter 7), the excess reactivity simulation of the shim rod was in very good agreement with the experimental value with a deviation of only 0,35%. The regulating rod was still in fair agreement deviating 6,91%. The comparison of the core excess simulation (2,267 \$) and the experimental results (2,220 \$) shows a final discrepancy of 2,10%, which is a very good agreement and strong validation of the simulations, performed throughout this thesis.

#### Excess Reactivity

		Experiment [\$]	Serpent (incl. Offset) [\$]	Serpent (excl. Offset) [\$]
Core I	Shim Rod	1,61	1,61	1,82
	Regulating Rod	1,06	1,06	1,15
	<b>Core Excess</b>	2,585	2,585	2,974
Core II+III	Shim Rod	1,63	1,65	
	Regulating Rod	0,73	0,72	
	<b>Core Excess</b>	2,360	2,369	
Core IV	Shim Rod	1,52	1,51	
	Regulating Rod	0,70	0,75	
	<b>Core Excess</b>	2,220	2,267	

Table 9.1: Summary of the results obtained in this thesis. The table shows the experimentally determined and the Serpent simulation excess reactivity of the Shim and the Regulating rod and the total core excess reactivity of the core configurations Core I, Core III and Core IV.

The final chapter of this thesis examined the time-evolution of U-235 in five representative fuel elements in every ring throughout all core configurations (see chapter 8). The amounts of burnup demonstrate that the fuel depletion is proportional to the duration of operation and the indirect proportional to the distance of the fuel element to the center of the core.

This plausible conclusions and the gained over all result for the core excess reactivity suggests, that Serpent is well suited to perform core calculations throughout core configurations that build on one another. Additionally it shows, that the considerations that went into the simulations were accurate and that the simplifications did not have a strong impact on the calculations.



## List of Figures

Figure 1.1:

<https://qph.ec.quoracdn.net/main-qimg-606e8cd36ed0dabed4e5acbc45d90915>

[Date: 2018-03-11]

Figure 1.2:

[https://phys.libretexts.org/TextMaps/General\\_Physics\\_TextMaps/Map%3A\\_University\\_Physics\\_\(OpenStax\)/Map%3A\\_University\\_Physics\\_III\\_\(OpenStax\)/10%3A\\_Nuclear\\_Physics/10.2%3A\\_Nuclear\\_Binding\\_Energy](https://phys.libretexts.org/TextMaps/General_Physics_TextMaps/Map%3A_University_Physics_(OpenStax)/Map%3A_University_Physics_III_(OpenStax)/10%3A_Nuclear_Physics/10.2%3A_Nuclear_Binding_Energy)

[Date: 2018-03-11]

Figure 2.2:

[https://www.ndc.jaea.go.jp/j40fig/jpeg/u235\\_f1.jpg](https://www.ndc.jaea.go.jp/j40fig/jpeg/u235_f1.jpg)

[Date: 2018-06-06]

Figure 2.3:

[https://www.uni-due.de/fb8/fbphysik/Hauptseminar/WS0506/Ausarbeitung\\_Kernspaltung.pdf](https://www.uni-due.de/fb8/fbphysik/Hauptseminar/WS0506/Ausarbeitung_Kernspaltung.pdf)

[Date: 2018-06-06]

Figure 2.4:

[https://www.researchgate.net/profile/Mark\\_Prelas/publication/262341758/figure/fig5/AS:296880786427906@1447793303193/U-235-fission-yields-for-high-and-low-energy-thermal-incident-neutrons-19.png](https://www.researchgate.net/profile/Mark_Prelas/publication/262341758/figure/fig5/AS:296880786427906@1447793303193/U-235-fission-yields-for-high-and-low-energy-thermal-incident-neutrons-19.png)

[Date: 2018-06-20]

Figure 2.5:

[https://media.springernature.com/original/springer-static/image/chp%3A10.1007%2F978-3-642-33846-5\\_3/MediaObjects/10279\\_2\\_De\\_3\\_Fig3\\_HTML.gif](https://media.springernature.com/original/springer-static/image/chp%3A10.1007%2F978-3-642-33846-5_3/MediaObjects/10279_2_De_3_Fig3_HTML.gif)

[Date: 2018-06-20]

Figure 2.6:

[http://www.tpub.com/doenuclearphys/nuclear%20physics%20and%20reactor%20theory\\_files/image617.jpg](http://www.tpub.com/doenuclearphys/nuclear%20physics%20and%20reactor%20theory_files/image617.jpg)

[Date: 2018-06-26]

Figure 2.7:

[https://ansn.iaea.org/Common/documents/Training/TRIGA%20Reactors%20\(Safety%20and%20Technology\)/chapter2/images/fig10.png](https://ansn.iaea.org/Common/documents/Training/TRIGA%20Reactors%20(Safety%20and%20Technology)/chapter2/images/fig10.png)

[Date: 2018-11-15]

Figure 3.1:

[https://ati.tuwien.ac.at/reactor/cross\\_section/EN/](https://ati.tuwien.ac.at/reactor/cross_section/EN/)

[Date: 2018-08-01]

Figure 3.2.:

Herzog, H.: "Development and Validation of a Serpent-2 model for the TRIGA Mark II reactor of the Technical University Vienna"/Master Thesis, Universität Wien 2017

Figure 3.4:

<http://www.rcp.ijs.si/ric/export/image5.gif>

[Date 2018-11-15]